IEEE Access
Multidisciplinary ⋮ Rapid Review ⋮ Open Access Journal

Received 13 February 2024, accepted 31 March 2024, date of publication 2 April 2024, date of current version 9 April 2024.

Digital Object Identifier 10.1109/ACCESS.2024.3384371

RESEARCH ARTICLE

Design and Implementation of Active Antennas for IoT-Based Healthcare Monitoring System

UMAR MUSA[1,3], (Student Member, IEEE), SHAHARIL MOHD SHAH[1], HUDA A. MAJID[1], (Member, IEEE), ISMAIL AHMAD MAHADI[2], (Graduate Student Member, IEEE), MOHAMAD KAMAL A. RAHIM[4], (Senior Member, IEEE), MUHAMMAD SANI YAHYA[5], (Graduate Student Member, IEEE), AND ZUHAIRIAH ZAINAL ABIDIN[1], (Senior Member, IEEE)

[1]Advanced Telecommunication Research Center (ATRC), Universiti Tun Hussein Onn Malaysia (UTHM), Batu Pahat, Johor 86400, Malaysia
[2]Faculty of Exact and Applied Science, University of N'Djamena, N'Djamena PB 1117, Chad
[3]Department of Electrical Engineering, Bayero University Kano, Kano 700006, Nigeria
[4]Advanced RF and Microwave Research Group, Faculty of Electrical Engineering, Universiti Teknologi Malaysia (UTM), Johor Bahru, Johor 81310, Malaysia
[5]Department of Electrical and Electronics Engineering, Abubakar Tafawa Balewa University, Bauchi 740272, Nigeria

Corresponding authors: Shaharil Mohd Shah (shaharil@uthm.edu.my), Ismail Ahmad Mahadi (ismailaht@ieee.org), and Umar Musa (ge210004@student.uthm.edu.my)

This work was supported by the Ministry of Higher Education (MoHE) under Fundamental Research Grant Scheme FRGS/1/2020/TK0/UTHM/02/44.

ABSTRACT This work presents the design and implementation of active antennas as a part of a healthcare monitoring system that is based on the Internet of Things (IoT). The monitoring system comprises a SEN11547 pulse sensor and an LM35 temperature sensor for measuring heart rate in Beats Per Minute (BPM) and body temperature in Degree Celsius (°C). This data is then sent to the ThingSpeak IoT platform, which necessitates the integration with the NodeMCU ESP-32S Wi-Fi module to ensure the availability of data. Two dual-band (2.4 GHz and 5.8 GHz) microstrip patch antennas, one with a PIN diode and one without, are fabricated using Rogers Duroid RO3003™ substrate. Both antennas have dimensions of 41 × 44 mm^2. In order to achieve a dual-band operation at 2.4 GHz, a slot in the shape of an inverted letter U is introduced, to the existing patch which generates a 5.8 GHz frequency band. By controlling the PIN diode's ON and OFF state, the active antenna can switch between a single band of 5.8 GHz and a dual-band of 2.4 GHz and 5.8 GHz. At both frequencies, the measured radiation patterns exhibit bidirectional and directional characteristics in the *E*-plane, whereas an omnidirectional pattern can be observed in the *H*-plane. In terms of nonlinear characteristics of the antenna, the third-order intermodulation distortion products (IMD3) frequencies are generated within an input power range of 0 to 20 dBm from the two-tone nonlinear measurements. Specifically, the IMD3 at 2.4 GHz is measured at −36.18 dBm and −47.19 dBm at 5.8 GHz. Additionally, the measurement showed that the 1-dB gain compression point (P_{1-dB}) was not detected at 2.4 GHz, indicating linear behavior within the RF input power range. However, at 5.8 GHz, the P_{1-dB} was observed at an RF input power level of 13.8 dBm, suggesting linear functionality up to this power level. The experimental data are obtained from ten participants with ages ranging between 18 and 40 years old for 10-minutes duration with a 1-minute step size which implies 10 samples. For comparison and validation, the measurements are compared with the commercially available Laird Connectivity 2.4GHz/5.8GHz dipole antenna. It can be observed that the heart rate ranges from 85 BPM to 92 BPM for the active antenna whereas for the reference antenna, the values range from 84 to 90 BPM, which implies a good agreement. On the other hand, the body temperature ranges from 29 to 37°C for the active antenna and from 30 to 36°C for the reference antenna, which infers a good agreement as well. Therefore, it is shown that the proposed dual-band active antennas in this work can be effectively integrated into the IoT-based healthcare monitoring system.

The associate editor coordinating the review of this manuscript and approving it for publication was Weiren Zhu.

INDEX TERMS IoT platform, healthcare monitoring, patch antenna, PIN diode, vital sign, sensor.

I. INTRODUCTION

Internet of Things (IoT) has integrated into contemporary society, serving as a platform for acquiring data and facilitating long-distance wireless communication [1], [2], [3]. In order to implement the IoT concept, multiple sensors are employed on the microcontroller to perform the required tasks and display the data on the IoT platform. The application of IoT technologies spans a wide range of fields, including healthcare systems for monitoring heartbeat, and body temperature, military operations, smart cities, smart homes, as well as agricultural applications [4], [5], [6], [7].

These applications aim to enhance resource allocation and overall efficiency. The Internet of Things (IoT) applications' general performance and device access to the Internet are being further improved by wireless network technologies [8]. An integral component within wireless sensor technology is the antenna, which plays a crucial role as IoT techniques continue to rapidly evolve, discovering more and more uses in a variety of industries, including monitoring, agriculture, intelligent cities, intelligent homes, and surveillance. The expanding need in communication technology for multi-frequency and multi-function antennas has led to significant attention being focused on the design of compact and easily integrated antennas in recent years [9].

In the realm of advanced wireless communication devices, there is a growing need for versatile antennas that can adapt to rapidly changing user requirements [10]. Traditional fixed antennas are insufficient to meet this demand. Depending on specific circumstances and limitations, it becomes necessary to modify antenna characteristics to ensure the delivery of high-quality services. Reconfigurable antennas are designed to address this need, as they can alter their frequency, radiation pattern, polarization, or any combination thereof [11], [12], [13], [14]. Numerous efforts have been dedicated to the development of reconfigurable antenna designs [15], [16], [17], [18], [19]. In order to achieve antenna reconfiguration, active devices are commonly employed, including PIN diodes, varactor diodes, and RF MEMS switches [20], [21], [22]. Varactor and PIN diodes offer advantages such as low insertion loss and seamless frequency band adjustments, but they exhibit nonlinear behavior. On the other hand, RF MEMS switches provide excellent isolation properties but are characterized by a slower switching speed [23], [24], [25].

Due to the nonlinear characteristics of active devices at high frequencies, when these devices are integrated into the antenna system, they exhibit nonlinear behavior that requires careful consideration to avoid impacting the performance of the front-end communication system [26]. Nonlinear components such as diodes and transistors offer significant advantages in applications involving amplification, detection, and frequency reconfiguration. However, they also possess undesirable traits, including gain compression and the generation of unwanted frequency components. These consequences can result in increased signal losses, distortion, and interference with other radio channels or services [27]. Consequently, it is essential to assess active antennas in terms of parameters such as intermodulation distortion (IMD) to understand their dynamic behavior. Higher frequencies are used to transmit mixed communication data; these frequencies fall between 2.4 and 5.8 GHz, which are unlicensed ISM bands.

Medical practitioners can benefit greatly from IoT-based healthcare applications including wellness examinations, which lower expenses, improve the standard of living, improve medical diagnosis, and make medical procedures easier [28]. Among the various health services, the monitoring of vital signs is of particular importance [29]. Prioritizing the monitoring of vital signs [30] stands as a critical imperative for healthcare institutions aiming to facilitate early prevention [31] and diminish mortality rates. Although medical practitioners employ conventional methods for assessing patients' vital signs within hospital settings, this equipment's reliance on traditional approaches [32] results in inherent inefficiencies concerning time. This situation distinctly impacts real-time patient healthcare services [33], particularly during the diagnostic phase of illnesses, leading to escalated operational expenses and augmented medical personnel workloads. IoT-based healthcare monitoring appears as an opportunity to improve the sector in real-time and get beyond the drawbacks of traditional healthcare devices [34]. Due to the presence of IoT-enabled health monitoring systems, individuals can now access essential physiological data from the comfort of their homes. This advancement notably benefits elderly patients, for whom the arduous journey to a medical facility can be both physically demanding and taxing.

Numerous researchers are actively exploring investigations on vital signs to diagnose various medical conditions. The implementation of the proposed designs encompasses the utilization of Arduino-based IoT technology to monitor heartbeats [35] and body temperature [36], [37]. Research findings indicate that data related to heartbeat diagnoses can be managed via smartphones [38] and computer servers [39], [40], [41]. Authors in [42] examine IoT-driven patient monitoring systems employing sensors for the identification, assessment, and continuous tracking of two fundamental vital signs. The system's architecture incorporates the Arduino Mega 2560, ESP8266 Wi-Fi Module, and two sensor modules to formulate an IoT-centered patient monitoring setup. This configuration proficiently detects core vital signs, namely body temperature and respiratory rate. Furthermore, it assesses these vital sign levels for the patient's age, delivers notifications for irregular conditions, and transmits the results wirelessly through Android applications. An alternative design, involving wearable IoT-enabled real-time healthcare monitoring systems [43], [44], [45], entails the development

of a wearable IoT-cloud-based healthcare monitoring framework tailored for continuous individual health surveillance.

This undertaking involves an assortment of wearable sensors, encompassing heartbeat and body temperature monitoring. Similarly, a review of IoT-based health monitoring systems, characterized by the integration of Raspberry Pi, LPC2129, and wearable biomedical devices [46], delves into IoT-driven health monitoring approaches employing the mentioned components. In [47], the authors propose a system for the measurement of body temperature and heart rate. Notably, across these various studies, heart rate and body temperature emerge as consistent focal points. In a separate study [48], the author presents a comprehensive system capable of measuring body temperature and heart rate, with the capacity to transmit this data to both a mobile application and a wearable device.

This proposed work introduces the design and implementation of active antennas for an IoT-based healthcare monitoring system. Two types of antennas: one with a PIN diode and one without, are fabricated using Rogers Duroid RO3003™ substrate. The antennas can be integrated into the wireless healthcare monitoring system that operates within the 2.4 and 5.8 GHz unlicensed ISM bands. The performance of a wireless healthcare monitoring system using active antennas is evaluated using both laboratory equipment and real-world operating scenarios, and they are compared against a dipole antenna as a benchmark.

The implemented system streamlines processes for patients, caregivers, physicians, and other healthcare professionals involved. It also automates the periodic measurement of vital signals for multiple patients, ensuring dependable healthcare services. Additionally, vital signals play a pivotal role in monitoring and deducing an individual's physiological condition. They offer valuable insights into overall health status and are indispensable for determining treatment plans and prioritizing care.

II. DESIGN AND CONFIGURATION OF THE ANTENNAS

In order to meet the requirements of this work, a dual-band antenna is designed and simulated in the initial stage. Two versions of the antenna: one with a PIN diode and one without are considered. The simulations are conducted using CST MWS®software, a finite integration-based 3D electromagnetic (EM) simulator. The dimensions of the antennas are calculated using the transmission line model theory outlined in [49]. Based on a recent study in [50], incorporating inset feeding and integrating slots into the radiating structure leads to enhanced compactness and bandwidth, along with the generation of additional resonant frequencies. The dual-band characteristics are achieved by the introduction of an inverted U-slot to the patch. Additionally, a partial ground plane and two smaller slots are included at the bottom edge of the patch to improve the antenna's bandwidth. For the proposed antenna with a PIN diode, a frequency reconfiguration technique is employed that allows it to switch

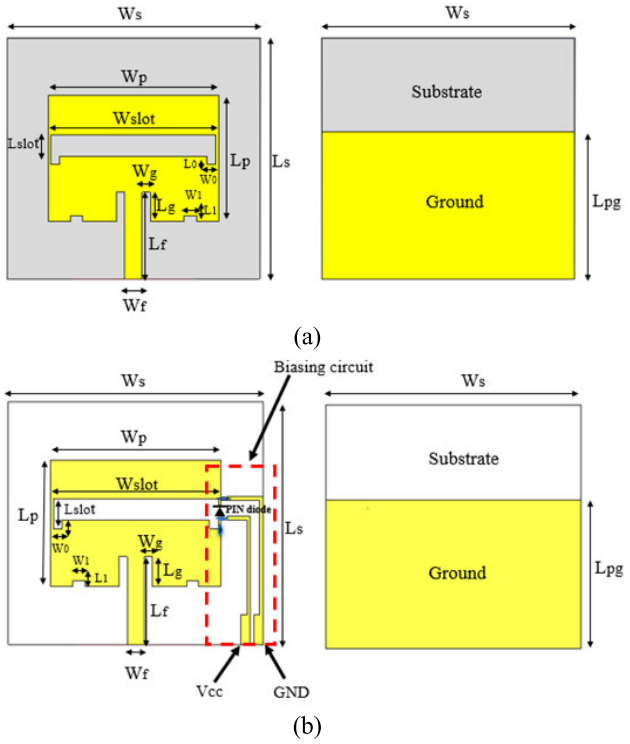

FIGURE 1. Active antennas geometry: (a) Without a PIN diode (b) With a PIN diode. Dimensions are Ls = 41 mm, Ws = 44 mm, Wp = 29 mm, Lp = 21 mm, Lpg = 25 mm, Wslot = 28 mm, Lslot = 3.7 mm, h = 1.52 mm, Wf = 2.98 mm, Lf = 15 mm, Lg = 5 mm Wg = 2 mm, Wo = 1.5 mm, Lo = 1.4 mm, W1 = 2.2 mm, L1 = 1 mm.

between the 2.4 GHz and 5.8 GHz of the ISM bands. Fig. 1 illustrates the design and geometry of the active antennas, both having dimensions of 41 × 44 mm^2. These antennas are fabricated on a Rogers Duroid RO3003™ substrate with specific properties (dielectric constant, $\varepsilon_r = 3$, thickness, h = 1.52 mm, and loss tangent, $\tan\delta = 0.0013$). The antennas are fed through microstrip lines connected to a central coaxial-fed sub-miniature version A (SMA) connector. Skyworks Technologies' SMP1321-079LF PIN diode is used [51] as an active device. This diode has a very low capacitance of 0.18 pF and operates within a frequency range of 10 MHz to 10 GHz. Fig. 2 shows the equivalent circuits of PIN diode and its detailed biasing circuit. In ON state, the diode exhibits series resistance and inductance values of R = 1.05 Ω and L = 0.7 nH, respectively as depicted in Fig. 2(a). In its OFF state, the diode is shunt configured with resistance and capacitance values of R = 2 kΩ and C = 0.18 pF, respectively as depicted in Fig. 2(b). The bias network, based on the design presented in [27], is used to control the PIN diode's operation. Fig. 2(c) depicts the PIN diode biasing network and its equivalent circuit. The values of the biasing circuit's inductor Lp = 27 nH and capacitor Cb = 1800 pF are chosen so that the biassing circuit and the RF line's impedance match. Whereas the inductor offers a conduit for the DC bias current needed for the PIN diode, the capacitor functions as insulation to avoid the DC bias current from damaging the RF signal.

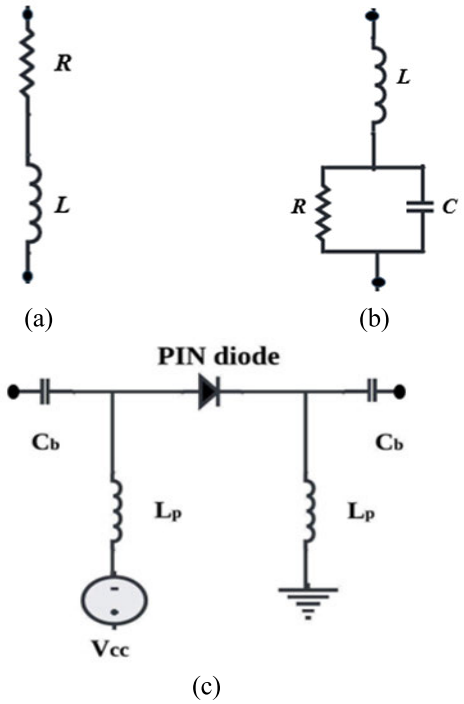

FIGURE 2. PIN diode lumped elements in (a) ON state (b) OFF state (c) detailed biasing circuit.

III. PERFORMANCE EVALUATION OF THE ANTENNAS

This section presents an investigation of the designed active antennas' functionality for IoT applications. Fig. 3 shows the fabricated antenna with Fig. 3(a) and (b) showcase the antenna without and with a PIN diode, respectively. N5234B Keysight Vector Network Analyzer (VNA) is employed for measuring the reflection coefficient (S_{11}) in dB, as illustrated in Fig. 4. The performances of the proposed antennas are assessed by comparing the simulated and measured S_{11}. The radiation patterns are measured in the anechoic chamber and are also compared with the simulations.

Fig. 5 compares the S_{11} between the antenna with and without a PIN diode. For the antenna without a PIN diode, as can be viewed in Fig. 5(a), The measured bandwidth at 2.4 GHz, which spans from 2.358 GHz to 2.447 GHz, is 3.8% (−10 dB). Similarly, the measured bandwidth at 5.8 GHz spans 5.2% (−10 dB) from 5.675 GHz to 5.975 GHz. The simulated and measured S_{11} findings have an acceptable agreement. Fig. 5(b) compares the measured and simulated S_{11} for the antenna with a PIN diode in ON and OFF states. The antenna functions at both 2.4 and 5.8 GHz while it is in ON state. At 2.4 GHz measures 3.8% (−10 dB) between 2.358 GHz to 2.447 GHz, while at 5.8 GHz measures 5.2% (−10 dB) from 5.675 GHz to 5.975 GHz. When the antenna is turned off, it functions at a single 5.8 GHz frequency band, with a measured bandwidth of 5.4% (−10 dB) spanning between 5.684 GHz to 5.989 GHz.

The assessment of antenna radiation involves analyzing 2D radiation patterns at each resonant frequency. The antenna's radiation patterns without a PIN diode are illustrated in

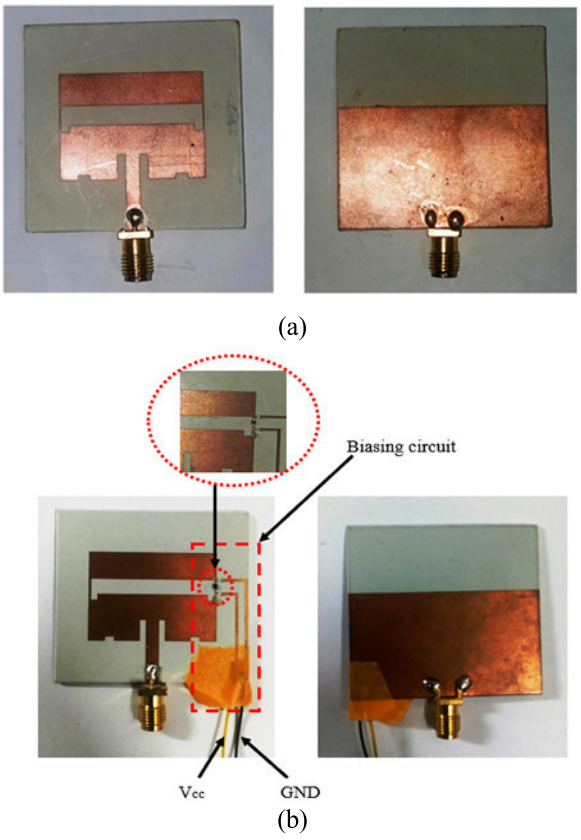

FIGURE 3. Fabricated active antennas: (a) Without a PIN diode (b) With a PIN diode.

Fig. 6. At 2.4 GHz, the E-plane exhibits bidirectional patterns, while the H-plane shows omnidirectional patterns as seen in Fig. 6(a). At 5.8 GHz, the E-plane patterns become directional, and the H-plane patterns remain omnidirectional as seen in Fig. 6(b). Additionally, Fig. 7 presents the 2D radiation patterns of the antenna with a PIN diode. In ON state, specific characteristics emerge at 2.4 GHz as seen in Fig. 7(a), the E-plane shows bidirectional patterns, and the H-plane exhibits omnidirectional patterns; at 5.8 GHz as seen in Fig. 7(b), the E-plane patterns are directional, and the H-plane patterns are omnidirectional. In OFF state, the antenna's behavior changes, with directional E-plane patterns at 5.8 GHz as seen in Fig. 7(c) and persistent omnidirectional H-plane patterns at the same frequency.

Fig. 8 shows the comparison between the simulated and measured gain and efficiency of the dual-band antenna without a PIN diode, the gain, G (dBi) was measured to be 3.73 dBi and 5.08 dBi at 2.4 GHz and 5.8 GHz which leads to efficiency, η (%) of 90% and 91.4% as shown in Fig. 8(a) and (b).

On the other hand, Fig. 9 shows the comparison between the simulated and measured gain and efficiency of the dual-band antenna with a PIN diode. In ON state, the gain, G (dBi) was measured to be 4.82 dBi and 5.75 dBi at 2.4 GHz and 5.8 GHz which leads to efficiency, η (%) of 90.1% and 87.4% as shown in Fig. 9(a) and (b). Whereas in

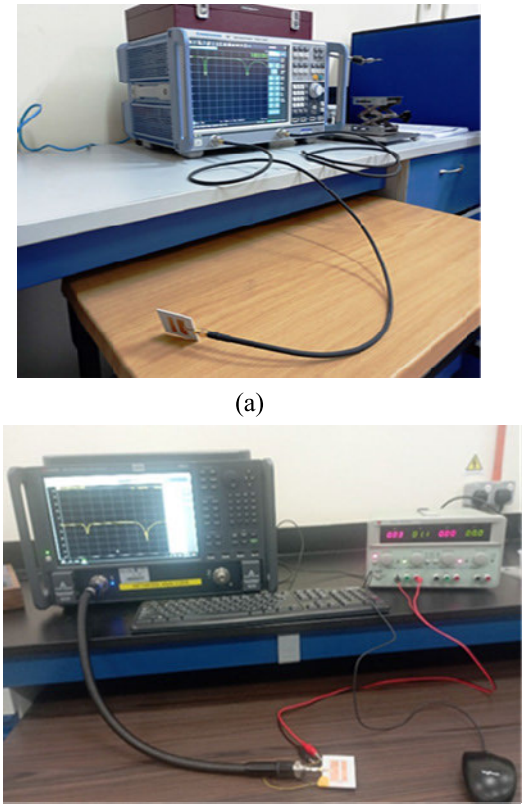

(a)

(b)

FIGURE 4. S11 measurement setup (a) Without a PIN diode (b) With a PIN diode.

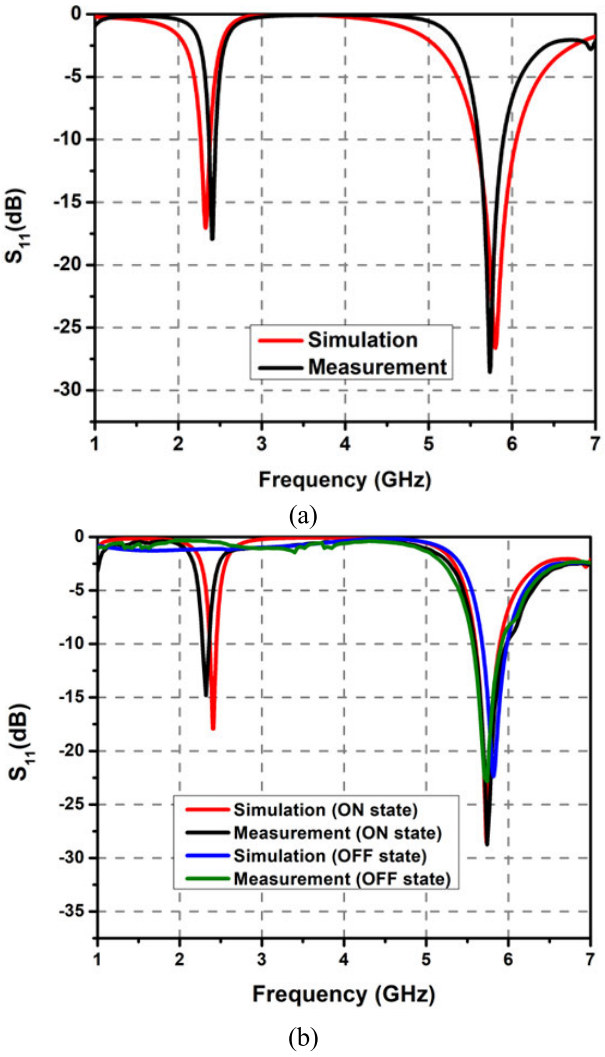

FIGURE 5. S11 comparison (a) Without a PIN diode (b) With a PIN diode.

OFF state, the gain, G (dBi) was measured to be 5.9 dBi at 5.8 GHz which leads to efficiency, η (%) of 90% as shown in Fig. 9(c).

In order to gain a deeper understanding of the operational principles behind the dual-band antenna without and with a PIN diode design, the current distribution diagrams at various resonant modes are examined and illustrated in Fig. 10. In Fig. 10(a), the current distribution of the antenna with the main radiating patch reveals concentration around the transmission line and the edges of the patch, emphasizing the crucial role of the main radiating patch in generating the resonant frequency of 5.8 GHz. Conversely, Fig. 10(b) demonstrates that at 2.4 GHz, the maximum current concentration occurs along the edges of the inverted U-slot. Fig. 11 depicts the current distribution of the antenna with a PIN diode. In ON state, the highest current concentration is evident along the edges of the slot at 2.4 GHz as seen in Fig. 11(a). In contrast, at 5.8 GHz, a significant current concentration is observed around the center of the main radiating patch as seen in Fig. 11(b). Fig. 12 further illustrates the current distribution of the antenna with a PIN diode in OFF state, focusing on 2.4 GHz and 5.8 GHz. In Fig. 12(a), during the OFF state, the current flow is minimal (barely noticeable) along the edges of the slot responsible for the 2.4 GHz. However, at 5.8 GHz, depicted in Fig. 12(b), a substantial current concentration is still noticeable around the center of the main radiating patch. The findings are consistent with the theoretical framework described in previous research [9], which asserts that the operating frequency is influenced by the current path length along the antenna's patch. Specifically, as the current path on the radiating structure of antennas extends, the resonant frequency decreases, and conversely, a shorter current path leads to a higher resonant frequency.

A. NONLINEARITY ANALYSIS OF THE ANTENNAS

PIN diodes demonstrate nonlinear characteristics when exposed to varying input power levels. This nonlinearity arises from the diode's operational state and the interaction between the RF signal and the diode's internal junction capacitance. Intermodulation distortion (IMD) products are multi-tone distortions resulting from the presence of two or more signals at the input of a non-linear device [52]. As the input power level increases, PIN diodes used for antenna reconfiguration exhibit nonlinear behavior, leading

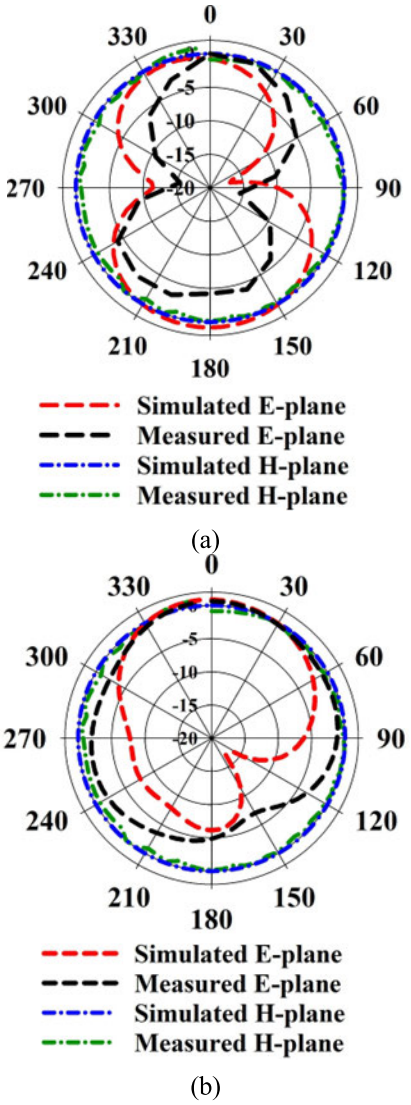

FIGURE 6. Radiation patterns without a PIN diode at (a) 2.4 GHz (b) 5.8 GHz.

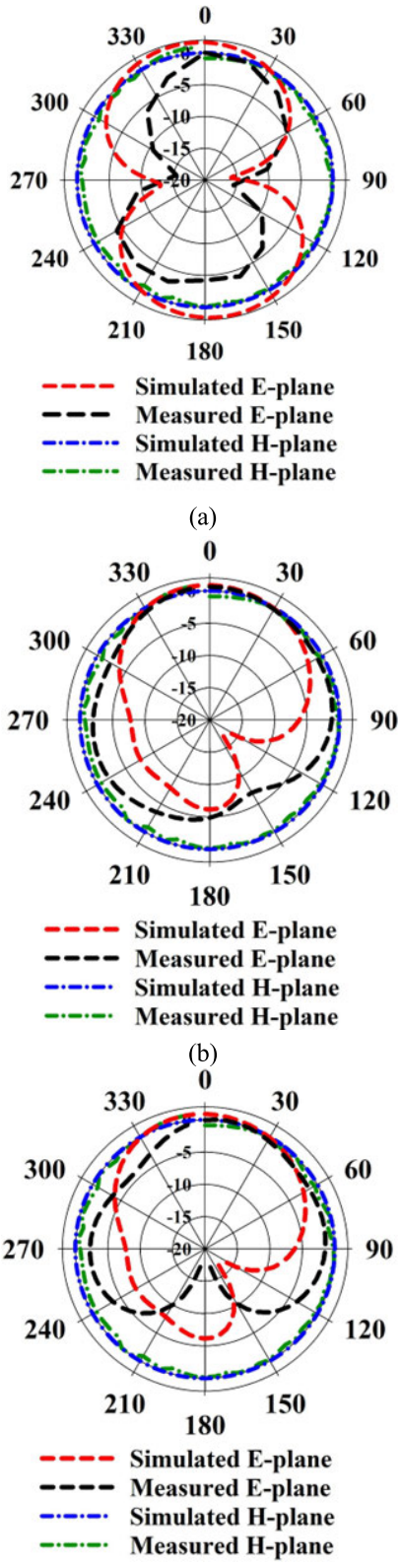

FIGURE 7. Radiation pattern with a PIN diode at (a) 2.4 GHz (ON state) (b) 5.8 GHz (ON state) (c) 5.8 GHz (OFF state).

to the generation of harmonics and intermodulation distortions. These nonlinear effects diminish the antenna's ability to handle high RF power and can potentially interfere with other systems. IMD products can either transmit or reflect through the feed network [53]. Antennas designed for indoor and short-range communication applications need to operate within frequency bands that can deliver output power levels of up to 30 dBm [36]. In such systems, active antennas must perform effectively at each power level with minimal distortion. Consequently, a comprehensive characterization process is essential for reconfigurable antennas, more so than for passive conventional antennas. Moreover, the 1-dB gain compression point, often referred to as P_{1-dB}, is a fundamental and widely used figure of merit in the nonlinear characterization of electronic devices and systems. It is another key indicator of a device's linearity and its ability to control the gain in the presence of varying input signal power levels. P_{1-dB} plays a crucial role in the design and performance assessment of active switches linearity performance [54]. This indicates that the input power is raised

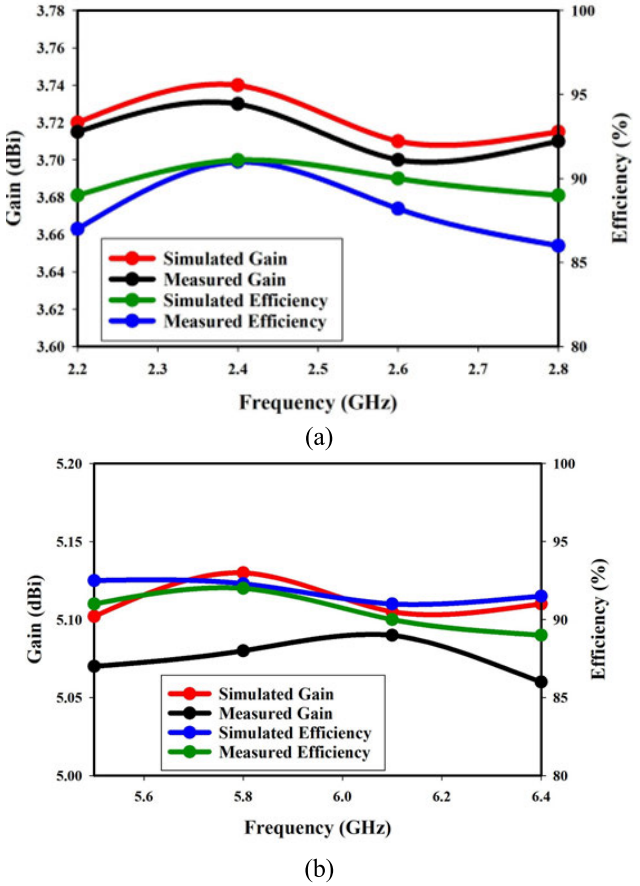

FIGURE 8. Simulated and measured gain and efficiency without a PIN diode at (a) 2.4 GHz (b) 5.8 GHz.

beyond the 1-dB point. The P_{1-dB} point also measures the dynamic range of the device, a crucial aspect for signal processing, communication systems, and various applications. A higher P_{1-dB} value suggests that the device can manage a broader input power range without experiencing significant gain compression or distortion. This is especially important in applications where signals with varying amplitudes need to be processed, as it ensures that the device can maintain linearity and signal fidelity. P_{1-dB} is typically determined experimentally by gradually increasing the input power and measuring the corresponding gain reduction. This measurement is often performed using network analyzers, spectrum analyzers, or specialized test setups [55].

The experimental setup used in this study to assess the nonlinear characteristics of the active antennas in transmitting mode is shown in Fig. 13. Initially, the generator's output power and power combiner's output power are measured to assess the losses that might be incurred in the cables. Subsequently, the power of radiated signals is measured using the commercial ETS 3106B horn antenna (reference antenna) positioned at 1 meter away from the active antenna as shown in Fig. 13(a). Horn antenna's orientation is changed to correspond with the antenna's polarization. The incoming signals are then displayed using a Keysight N9951A spectrum

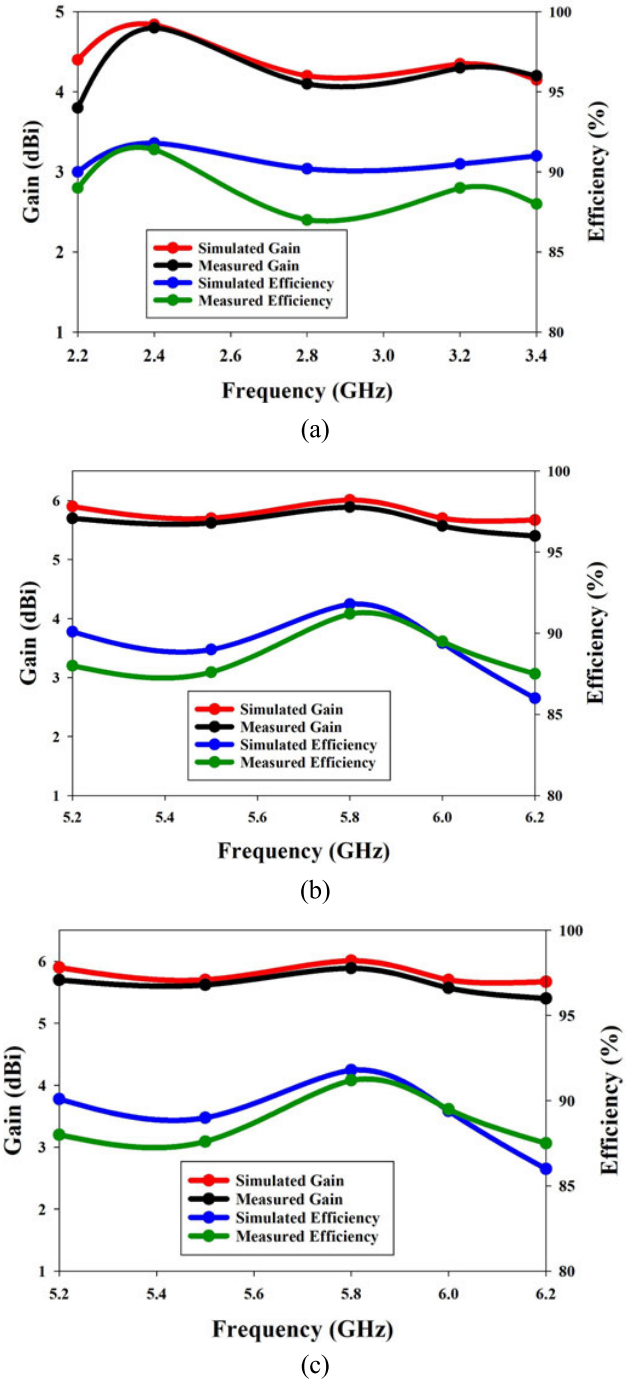

FIGURE 9. Simulated and measured gain and efficiency with a PIN diode at (a) 2.4 GHz (ON state) (b) 5.8 GHz (ON state) (c) 5.8 GHz (OFF state).

analyzer to identify the received signal power. Fig. 13(b) illustrates the experimental setup for measuring the P_{1-dB}. The received power of the transmitted signals is produced across a range of input power levels, spanning from 0 to 20 dBm at the specified IMD3 frequency. The determination of P_{1-dB} involves identifying the point on the graph plotting received power against input power where the output power experiences a 1 dB decrease. Nonlinearity assessments are

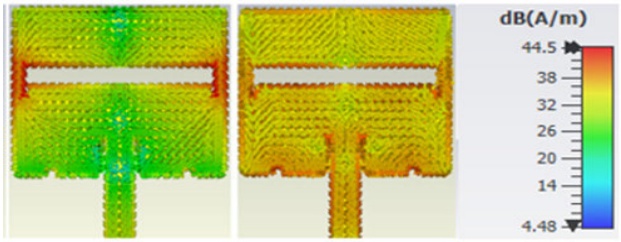

FIGURE 10. Current distribution without a PIN diode at (a) 2.4 GHz (b) 5.8 GHz

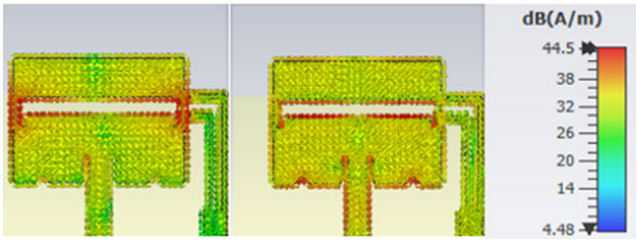

FIGURE 11. Current distribution with a PIN diode in ON state at (a) 2.4 GHz (b) 5.8 GHz

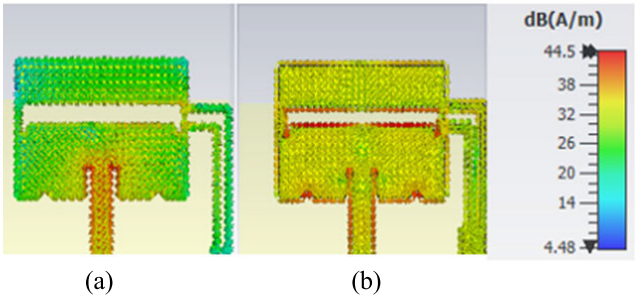

FIGURE 12. Current distribution with a PIN diode in OFF state at (a) 2.4 GHz (b) 5.8 GHz

conducted in the laboratory for the proposed active antenna, as depicted in Fig. 13(c).

Prior to the nonlinearity measurement, the S_{11} of the antenna is measured based on the input power from 0 dBm to 20 dBm. The behavior of the active antenna starts to change as the RF power increases. Consequently, the antenna's impedance undergoes variations with changing input power levels, leading to a degradation in impedance matching and resulting in higher S_{11} values. Fig. 14 shows the S_{11} for each input power level. When the RF input power reaches 20 dBm, the antenna operates within the linear region. However, the changes in S_{11} are relatively minor, with only negligible fluctuations observed beyond the 15 dBm power level, which implies that the presence of a PIN diode will not affect the S_{11} of active antennas in this work.

Another crucial aspect associated with the device's nonlinearity is the potential for IMD3 products, which can lead to signal distortion and interference with various systems or channels featuring closely spaced carriers. Hence, it becomes imperative to investigate harmonic distortions for nonlinear circuits, given that the proposed antenna operates in two modes: a single-band mode of 5.8 GHz and a dual-band mode of 2.4 GHz and 5.8 GHz. In this scenario, a two-tone input signal is employed, consisting of two closely spaced tone signals: $f_1 = 2.399$ GHz and $f_2 = 2.401$ GHz for the 2.4 GHz band, and $f_1 = 5.799$ GHz and $f_2 = 5.801$ GHz for the 5.8 GHz band. These two-tone signals are combined using a power combiner, and the proposed antenna receives the resulting mixed two-tone signals. A horn antenna ranging from 1 to 6 GHz is utilized, followed by a spectrum analyzer to detect the fundamental signals and intermodulation products. The power of the two-tone RF signal is incrementally increased from 0 dBm to 20 dBm, with the analysis focusing on two cases at different power levels (10 dBm and 20 dBm). For an input power level of 10 dBm at 2.4 GHz, the received signal strength for the primary signals is recorded at −11.86 dBm and −10.56 dBm, respectively. In Fig. 15(a), it's evident that the received signal strengths for IMD3 are notably lower than the standard noise level of −70 dBm at this power level. When the RF input power to the antenna reaches 20 dBm at 2.4 GHz, asymmetric IMD3 products become evident at 2.397 GHz and 2.403 GHz, registering values of −36.18 dBm and −34.32 dBm, respectively. Both of these values are observable and exceed the noise level. In contrast, the strengths of the fundamental signals are 11.22 dBm and 11.3 dBm, as seen in Fig. 15(b).

At an input power level of 10 dBm at 5.8 GHz, the received signal strength for the primary signal measures −15.67 dBm and −15.37 dBm, respectively. Fig. 16(a) illustrates that the received signal strengths for IMD3 remain below the standard noise level of −70 dBm at this power level. When the RF input power to the antenna is elevated to 20 dBm at 5.8 GHz, you can also detect asymmetric IMD3 products at 5.797 GHz and 5.803 GHz, measuring −31.5 dBm and −47.19 dBm, respectively. These values are both discernible and surpass the noise level. In contrast, the strengths of the fundamental signals are 7.91 dBm and 8.1 dBm, as illustrated in Fig. 16(b). Based on the nonlinearity measurement, it is hence demonstrated that the active antennas in this study function in the linear region up to an input power level of 15 dBm, when the received signal intensity of the IMD3 is negligible.

In order to find the P_{1-dB}, a single-tone input signal of 2.4 GHz and 5.8 GHz were used. Fig. 17 shows the P_{1-dB} at 2.4 GHz and 5.8 GHz. The P_{1-dB} could not be found at 2.4 GHz as shown in Fig. 17(a), which implies that the antenna behaves linearly within the range of RF input power levels. Conversely, the P_{1-dB} can be observed at 5.8 GHz with a value of 13.8 dBm of RF input power level as can be viewed in Fig. 17(b). Hence, the antenna functions linearly up to 13.8 dBm input power.

The nonlinearity measurement results of the dual-band antenna with a PIN diode are also compared with the previous work in terms of size, substrate material, type of reconfigurations, gain, IMD3 products and P_{1-dB}, which can be

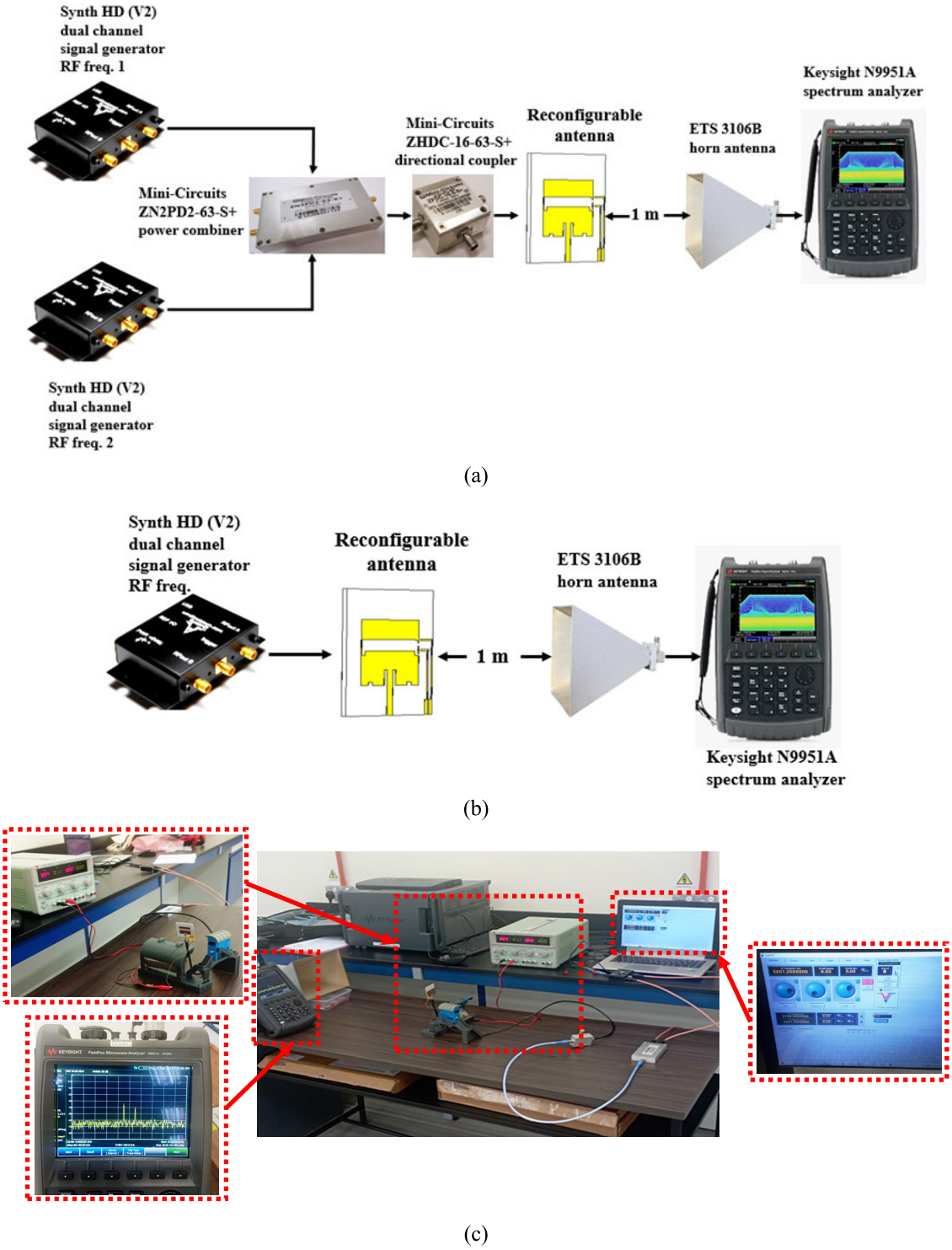

FIGURE 13. Experimental setup to measure the nonlinearity of active antennas (a) IMD3 products (b) P1-dB (c) The laboratory setup.

seen in Tab. 1. From the table, the proposed antenna in this work has a compact size of 41 × 44 mm^2 and high gain at both frequency bands. Moreover, the proposed antenna only uses a single switch, which reduces the antenna's complexity.

IV. IoT-BASED HEALTHCARE MONITORING SYSTEM

The objective of the proposed medical monitoring system is to gauge a patient's body temperature and heart rate, which are shown on the ThingSpeak application. The system hardware specifications define the features and services that the

TABLE 1. Comparison of this work and previous work in the literature in terms of nonlinearity measurements.

Ref.	Size (mm^2)	Material	Type of reconfigurations	Number of switches	Freq. (GHz)	Gain (dBi)	IMD3 products (dBm)	$P_{1\text{-}dB}$ (dBm)
[56]	60 × 60	FR-4	Radiation pattern	3	2.4	4.76	-19.3	30
[57]	20 × 28.5	Arlon	Frequency	1	2 / 2.4	2.15 / 2.8	NA / -18.5	NA / 14
[58]	50 × 20	Glass	Frequency	1	2	NA	-12.8	NA
[59]	65 × 65	Alumina	Frequency	12	3.2 / 3.5	6.5	NA / -35	NA / 20
[60]	150 × 75	Rogers RO5880™	Frequency	2	0.8 / 1.05	NA	-55 / -60	NA
This work	**41 × 44**	**Rogers RO3003™**	**Frequency**	**1**	**2.4 / 5.8**	**4.82 / 5.75**	**-36.18 / 47.19**	**NA / 13.8**

Note: A – Available; NA – Not available

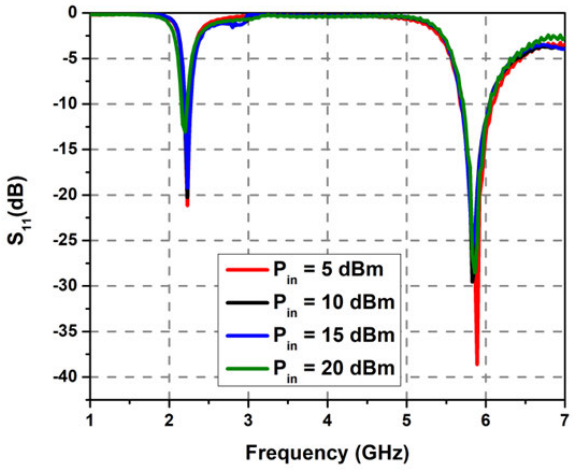

FIGURE 14. The measured S11 at different input power levels.

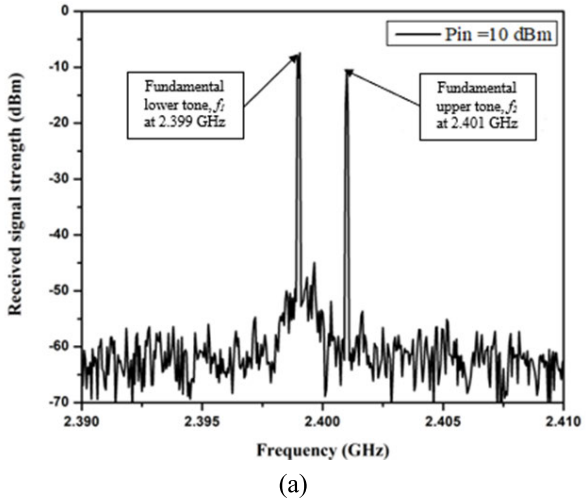

(a)

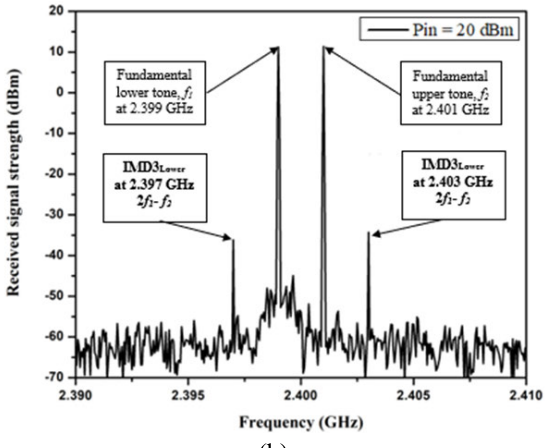

(b)

FIGURE 15. Received signal strength at 2.4 GHz (a) Pin=10 dBm (b) Pin=20 dBm.

healthcare monitoring system shall provide, as well as the limitations that it must work within. Defining the system requirements assists in making better component choices and optimizing resources.

A. PROPOSED SYSTEM CONFIGURATION

A functional prototype model is developed with a SEN11547 pulse sensor and LM35 temperature sensor from Spark Fun Electronics for measuring heartbeat and body temperature. Prominent vital indicators that indicate the state of processes that support life and the extent of medical conditions are body temperature and heart rate. Once the vital parameters are measured, they are transmitted and stored in the database of the ThingSpeak application through a NodeMCU ESP-32S Wi-Fi module connected to the active antennas for further analysis or long-term storage which might benefit the patients and medical personnel. The proposed healthcare monitoring system is illustrated in Fig. 18, called VITALS. The main objective of VITALS is to automate the measurement of vital signals, leading to improved healthcare services. Fig. 18(a) illustrates the complete block diagram of the healthcare monitoring system. From the figure, it can be seen that the healthcare monitoring system is controlled by a NodeMCU ESP-32S Wi-Fi module connected to the active antennas as the main controlling unit. The key components, which are

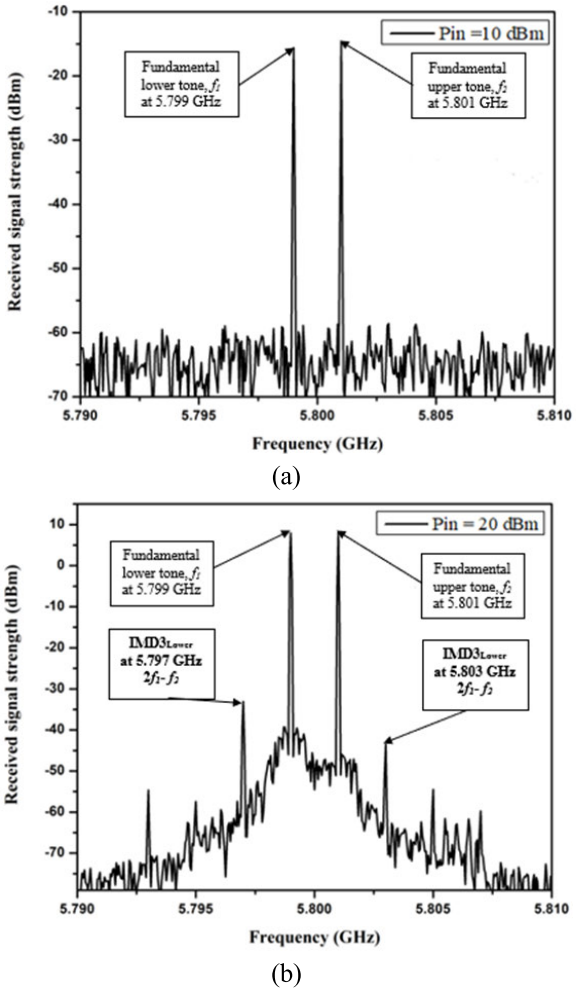

FIGURE 16. Received signal strength at 5.8 GHz (a) Pin=10 dBm (b) Pin=20 dBm.

the SEN11547 pulse sensor and LM35 temperature sensor these inputs will send signals to the microcontroller to be analyzed and processed. Open-source Arduino IDE software is employed, which is compatible with multiple operating systems. It facilitates uploading sketches to the prototype and retrieving data from the pulse sensor and temperature sensor through the serial monitor. The processed signals will then be sent to the output which includes the I2C Serial Interface 1602 LCD module, and they are transmitted and stored in the database of the ThingSpeak application. Fig. 18(b) illustrates the complete circuit diagram of the health care monitoring system featuring active antennas. This circuit is driven by the NodeMCU ESP-32S Wi-Fi module, which has an external antenna connected to pin 35 (GPI01/TX0) of the NodeMCU ESP-32S module. Power is supplied to the NodeMCU ESP-32S module through a 12-V DC adapter. However, in the event of a power supply failure, a battery can act as a reliable backup power source. The system includes an LCD display connected to the I2C module, which contains SDA, and SCL connected to pin 33 (GPI021) and pin 36 (GPI022) respectively, for displaying the output results. For heart rate monitoring, the pulse sensor incorporates an integrated optical amplification circuit and a noise-reducing circuit sensor, making it suitable for clipping onto the earlobe or fingertip and interfacing with the NodeMCU-32S module. The pulse sensor has three pins: VCC, GND, and an analog pin connected to pin 5 (GPI034). Additionally, the system incorporates the LM35 temperature sensor, which provides an analog response proportional to the current temperature. The output voltage can be directly translated into Celsius temperature values. In order to program and control the NodeMCU ESP-32S Wi-Fi module. The LM35 temperature sensor has three pins: VCC, GND, and an analog pin connected to pin 6 (GPI035).

B. PERFORMANCE EVALUATION OF THE SYSTEM

The IoT-based wireless healthcare monitoring system in this work, known as VITALS, is shown in Fig. 19. The circuit connections of VITALS when viewed internally is shown in Fig. 19(a), whereas Fig. 19(b) depicts the final product of VITALS. The monitoring system which utilizes different types of antennas is shown in Fig. 20. The experimental setup of VITALS using a dual-band antenna (without and with a PIN diode) and a commercial Laird Connectivity dipole antenna as the reference antenna can be viewed in Fig. 20(a) - (c), respectively. The microcontroller processes medical data, and the resulting signals are sent to the output, displayed on the I2C Serial Interface 1602 LCD module. Concurrently, the data is transmitted to the ThingSpeak application and stored in its database.

In order to conduct the experiment, ten participants, with their ages ranging between 18 and 40 years old, are selected to measure their heartbeats and body temperatures using the proposed system. The data of the ten participants are measured for 10 minutes duration with a 1-minute step size which implies 10 samples, under relaxed conditions or while they are not engaging in any physical activities. For comparison and validation, the measurements are compared with the reference antenna.

Graphical representations of patient vital signs can be viewed in Fig. 21. Fig. 21(a) - (j) illustrates the heart rate and body temperatures of ten volunteers which consists of data obtained from the healthcare monitoring system using the reference antenna and the proposed active antennas, without and with a PIN diode. From the figures, it can be observed that the heart rate of the volunteers ranges from 72 to 96 BPM which shows that despite variations in heart rate, all the recorded values remain within the normal range for an adult, which is between 60 and 100 BPM [61].

Moreover, the collection of body temperature data is carried out to assess the patient's body temperature condition. A rise in body temperature correlates with an increase in heart rate, while a decrease in body temperature corresponds to a decrease in heart rate. The temperature ranges from 30.20 to 37.80 °C, indicating a healthy range for an adult which is between 35 and 38 °C [61]. However,

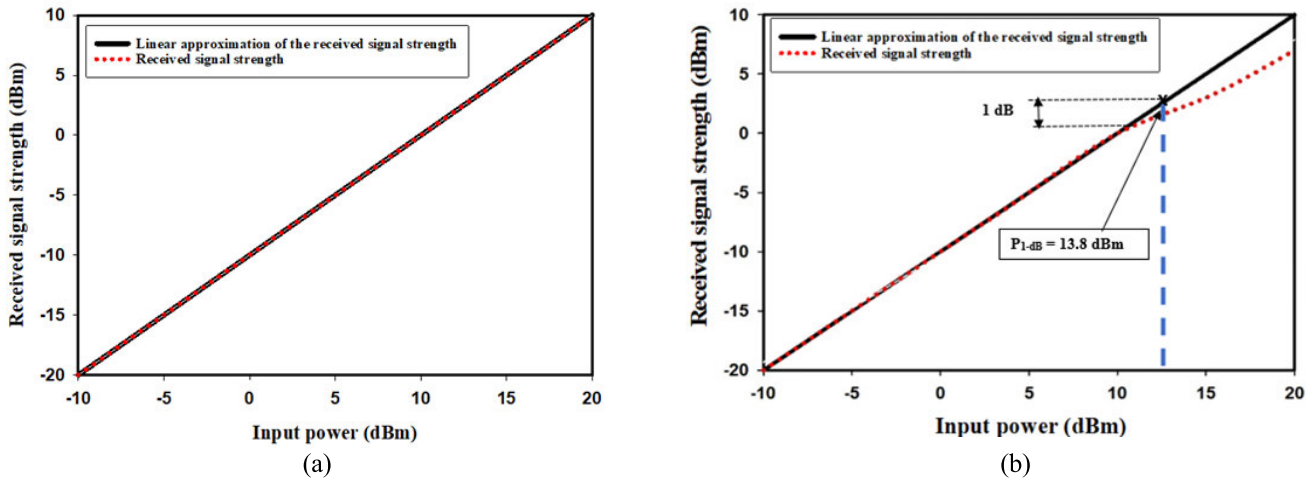

FIGURE 17. Measured 1-dB gain compression point of the dual-band antenna with a PIN diode: (a) 2.4 GHz (b) 5.8 GHz.

TABLE 2. Comparison of the heart rate and body temperature obtained from ten volunteers using the proposed healthcare monitoring system with various antennas.

Name	Age	Antenna without a PIN diode	Antenna with a PIN diode		Dipole antenna (Reference antenna)	Antenna without a PIN diode	Antenna with a PIN diode		Dipole Antenna (Reference antenna)
			ON State	OFF State			ON State	OFF State	
		Average heart rate (BPM)	Average heart rate (BPM)	Average heart rate (BPM)	Average heart rate (BPM)	Average body temperature (°C)	Average body temperature (°C)	Average body temperature (°C)	Average body temperature (°C)
Vol. A	25	88.9	89.3	86.6	88	34.3	34.5	34.5	34.1
Vol. B	19	91.4	89.2	86.5	88.5	35.6	35.3	33.8	36.2
Vol. C	18	85.5	86.2	81.3	84.1	31.4	30.4	31.7	32.3
Vol. D	32	87.3	89.6	85.5	87.7	36.4	35.5	33	37.1
Vol. E	38	88.7	88.8	86.6	88.8	29.6	33	32.3	29.9
Vol. F	30	87.8	87.5	85.8	88.1	33.9	34.2	34.1	33.7
Vol. G	18	88.7	88.5	85.8	84.4	30.6	32.1	31.7	29.8
Vol. H	25	91.4	89.1	86.5	85.3	34.6	35	32.3	35.3
Vol. I	28	86.7	87.5	84.7	85.2	30.9	30.3	30.1	31.3
Vol. J	20	89.3	89.2	88.2	89.7	34.3	34.8	33.9	33.8

it is worth noting that some values might fall below or slightly above this range, which could be due to factors like individual variability, recent activities, or environmental conditions.

The acquired data is subjected to analysis by computing the average values. In this context, the tabulated readings are presented in Tab. 2. This comparison serves to assess the accuracies of those antennas. From the table, the average heart rate measurements were taken across different conditions for three different antennas: the active antenna without a PIN diode, the active antenna with a PIN diode, and the commercially available Laird Connectivity antenna. The observed heart rates ranged from 85.5 BPM to 89.7 BPM for the active antenna without a PIN diode, 86.2 to 89.7 BPM for the active antenna with a PIN diode, and 88 to 89.7 BPM for the reference antenna. These results suggest that all three antennas provide consistent heart rate measurements, with minimal variation in the observed values. The close alignment of values between the active antennas and the reference antenna demonstrates the reliability and accuracy of the active antenna system, both with and without the PIN diode. Similarly, body temperature measurements were recorded under different conditions for the three antennas. The temperature range for the active antenna without a PIN diode was from 29.6 to 35.6°C, while for the active antenna with a PIN diode, it ranged from 30.4 to 35.5°C. In contrast, the reference antenna showed a slightly wider range, from 29.8 to 37.1°C. The overlapping temperature ranges for the active

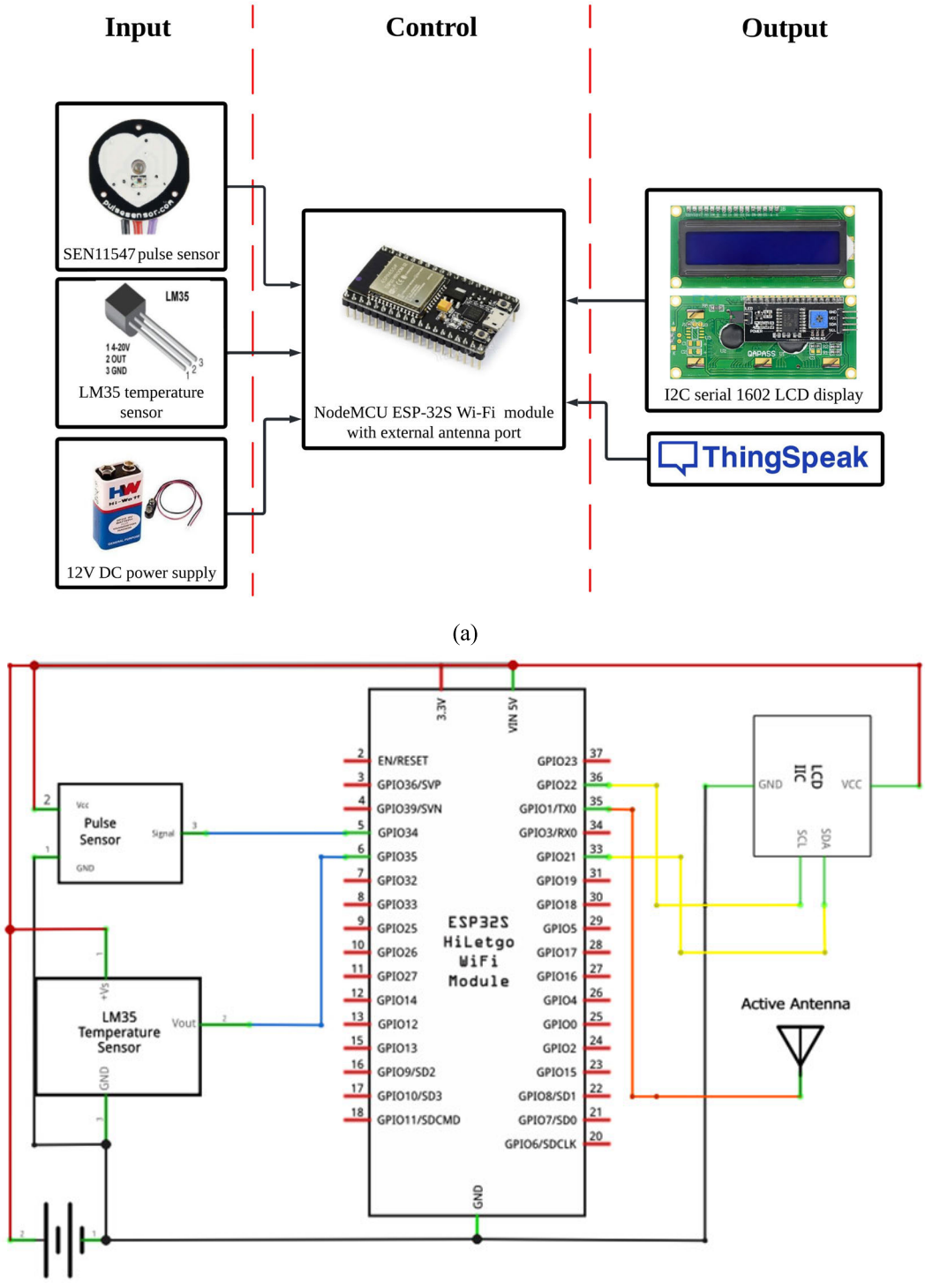

FIGURE 18. The proposed healthcare monitoring system called VITALS (a) Block diagram (b) Circuit diagram.

antennas and the reference antenna indicate that all three antennas provide consistent and comparable body temperature measurements. Overall, the results of this analysis show a strong agreement between the measurements obtained using the active antennas (both with and without the PIN diode) and the commercially available Laird Connectivity antenna. Minor variations in temperature ranges can be ascribed to factors such as antenna design or measurement conditions.

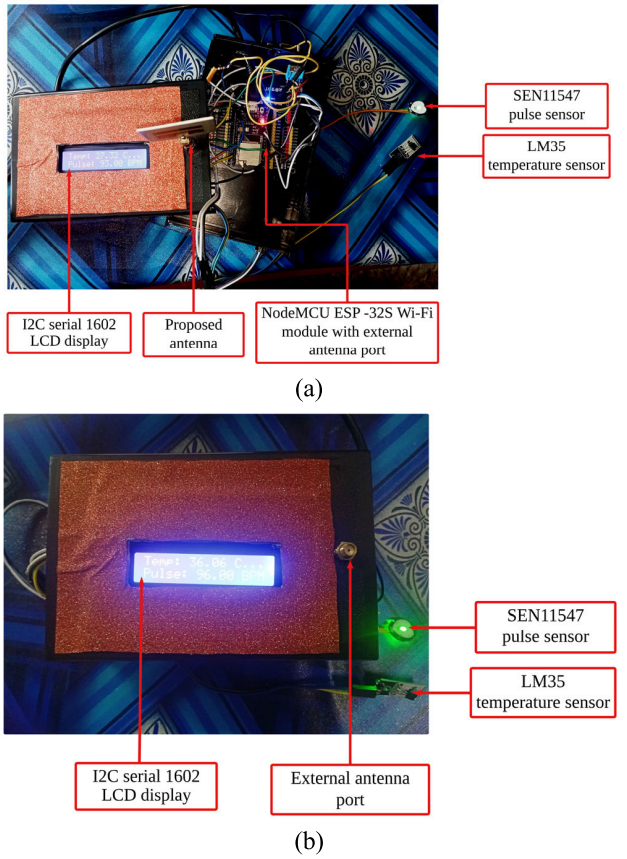

FIGURE 19. VITALS: (a) circuit connection when viewed internally (b) final product.

However, these differences do not markedly impact the overall accuracy and utility of the active antennas. In addition, the 10-minute time intervals can be considered sufficient based on the data obtained. This approach enables healthcare professionals to detect subtle changes, respond to emergencies, and provide tailored care, ultimately improving patient outcomes.

The current IoT-based wireless healthcare monitoring system and the IoT wireless healthcare monitoring system with dual-band active antennas are compared in Tab. 3. In contrast to all of the designs, the comparison demonstrates that the suggested antenna has a satisfactory gain and efficiency. The comparison table makes it clear that the majority of the current antenna dimensions are greater than those of the suggested active antennas. In contrast, the suggested antenna's performance has been tested in an IoT application running in real-time. According to the table, the suggested antenna performs better than the others, making it a suitable option for IoT applications. The primary benefit of the suggested IoT wireless healthcare monitoring system is its effective integration of dual-band active antennas appropriate for IoT applications.

FIGURE 20. The experimental setup of VITALS using different types of antennas: (a) antenna without a PIN diode (b) antenna with a PIN diode (c) commercial Laird Connectivity dipole antenna as a reference antenna.

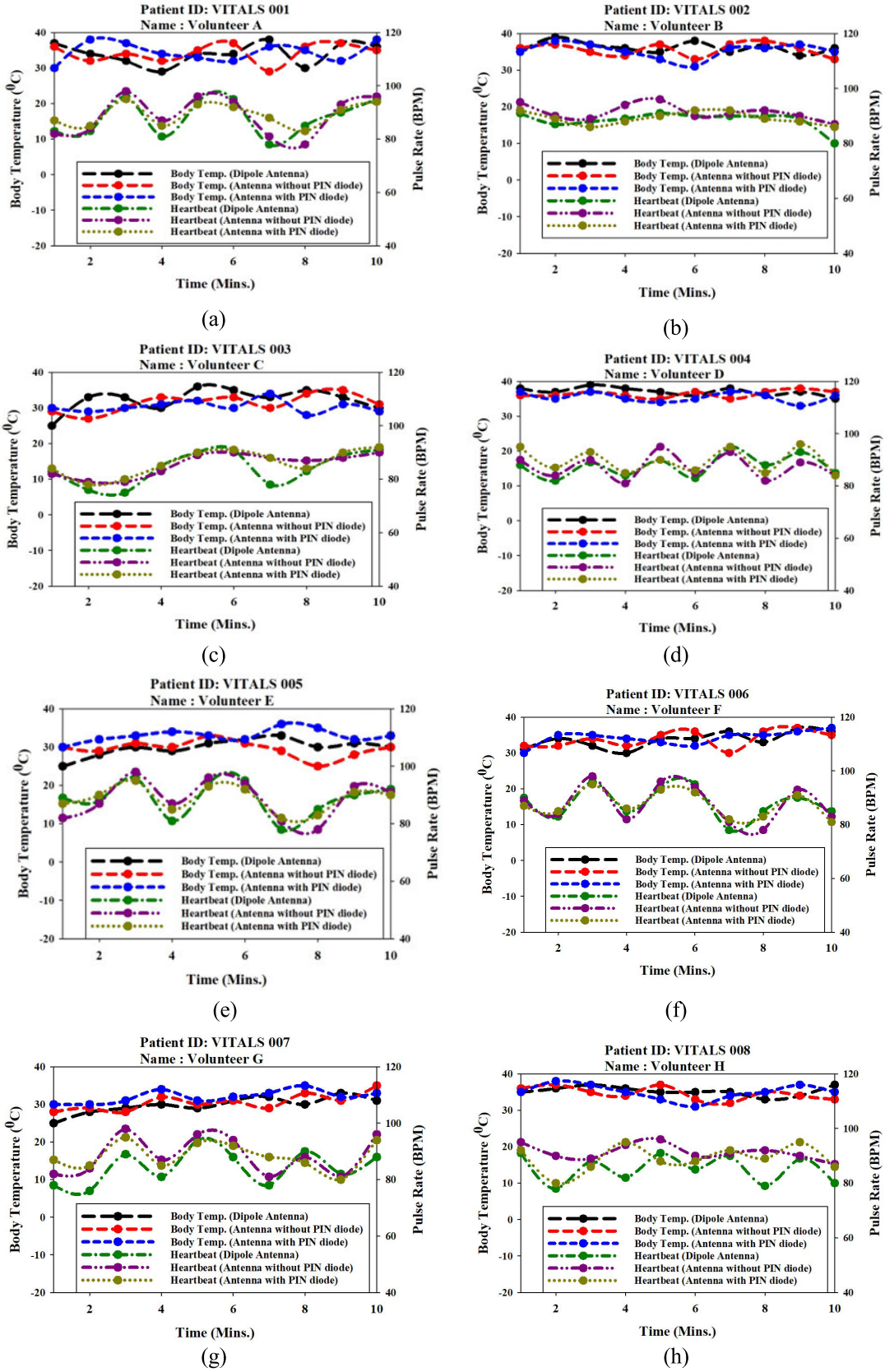

FIGURE 21. Comparisons of volunteers' heart rate and body temperature using various antennas (a) vol. A (b) vol. B (c) vol. C (d) vol. D (e) vol. E (f) vol. F (g) vol. G (h) vol. H.

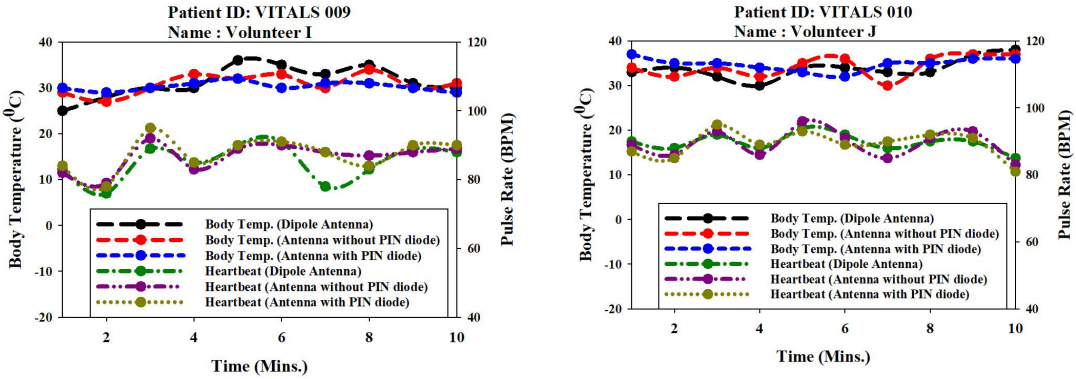

FIGURE 21. *(Continued.)* **Comparisons of volunteers' heart rate and body temperature using various antennas (i) vol. I (j) vol. J.**

TABLE 3. Comparison of the IoT-based wireless healthcare monitoring system currently in use and the IoT-enabled wireless healthcare monitoring system utilizing dual-band active antennas.

Ref	Size $(mm)^2$	Material (Type)	Electronic Circuit	Freq. (GHz)	Gain (dBi)/ Efficiency (%)	Application IoT	Proposed antenna used in the system
[62]	45 × 45	Thick Felt (Flexible)	A	2.4 / 5.8	2.1 / 2.2 65.1 / 75	Yes	Yes
[63]	40 × 40	PDMS (Flexible)	NA	2.4 / 5.8	0.7 / 0.9 43.8 / 73.8	No	No
[64]	150 × 95	FR-4 (Rigid)	A	2.4	1.722 82.7	Yes	Yes
[65]	120 × 65	FR-4 (Rigid)	A	2.4 / 5.8	2.9 / 3.2 NA	Yes	Yes
[66]	40 × 10	FR-4 (Rigid)	A	2.4	1.347 79	Yes	Yes
[67]	90 × 90	Polyester (Flexible)	A	2.4	6.47 62	No	No
[68]	80 × 80	Rogers (Flexible)	NA	2.4 / 5.8	1.1 / 4.5 90 / 84	No	No
This Work	**41 × 44**	**Rogers (Flexible)**	**A**	**2.4 / 5.8**	**4.82 / 5.75 90 / 91.4**	**Yes**	**Yes**

Note: A – Available; NA – Not available

V. CONCLUSION

This work introduces the design and implementation of active antennas within a healthcare monitoring system for IoT applications. This monitoring system incorporates a SEN11547 pulse sensor and an LM35 temperature sensor to capture heart rate and body temperature data. These measurements are then transmitted to the ThingSpeak IoT platform, necessitating integration with the NodeMCU ESP-32S Wi-Fi module to ensure data availability. Two dual-band microstrip patch antennas, each measuring 41 × 44 mm^2, were constructed on Rogers Duroid RO3003™ substrate. One of these antennas is equipped with a PIN diode, while the other is not. To achieve dual-band operation at 2.4 GHz and generate a 5.8 GHz frequency band, a slot in the shape of an inverted letter U is introduced to the existing patch. The active antenna can switch between a single 5.8 GHz band and a dual-band configuration of 2.4 GHz and 5.8 GHz by controlling the state of the PIN diode. Radiation patterns are measured at both frequencies, showing bidirectional and directional characteristics in the *E*-plane, while the *H*-plane exhibits an omnidirectional pattern. Nonlinear characteristics are evaluated, with IMD3 generated within an input power range of 0 to 20 dBm in two-tone nonlinear measurements. Specifically, IMD3 at 2.4 GHz is measured at −36.18 dBm, and at 5.8 GHz, it is measured at −47.19 dBm. Moreover, the measurements indicate that the P_{1-dB} was not detected at 2.4 GHz, suggesting linear behavior within the RF input power range. However, at 5.8 GHz, the P_{1-dB} is noted at an RF input power level of 13.8 dBm, indicating linear functionality up to this threshold. Experimental data are collected from ten participants aged between 18 and 40 years for a duration of 10 minutes with 1-minute intervals, resulting in 10 samples. To validate the results, measurements are compared to a commercially available Laird

Connectivity 2.4GHz/5.8GHz dipole antenna. The heart rate ranged from 85 BPM to 92 BPM for the active antennas and from 84 to 90 BPM for the reference antenna, demonstrating good agreement. Similarly, body temperature ranged from 29 to 37°C for the active antennas and from 30 to 36°C for the reference antenna, confirming strong agreement. Consequently, this study highlights the effective integration of the proposed dual-band active antenna into an IoT-based healthcare monitoring system.

REFERENCES

[1] A. Lavric, A. I. Petrariu, P.-M. Mutescu, E. Coca, and V. Popa, "Internet of Things concept in the context of the COVID-19 pandemic: A multisensor application design," *Sensors*, vol. 22, no. 2, p. 503, Jan. 2022, doi: 10.3390/s22020503.

[2] A. Rejeb, K. Rejeb, H. Treiblmaier, A. Appolloni, S. Alghamdi, Y. Alhasawi, and M. Iranmanesh, "The Internet of Things (IoT) in healthcare: Taking stock and moving forward," *Internet Things*, vol. 22, Jul. 2023, Art. no. 100721, doi: 10.1016/j.iot.2023.100721.

[3] Z. Qian, Y. Lin, W. Jing, Z. Ma, H. Liu, R. Yin, Z. Li, Z. Bi, and W. Zhang, "Development of a real-time wearable fall detection system in the context of Internet of Things," *IEEE Internet Things J.*, vol. 9, no. 21, pp. 21999–22007, Nov. 2022, doi: 10.1109/JIOT.2022.3181701.

[4] A. Khalifeh, K. A. Darabkh, A. M. Khasawneh, I. Alqaisieh, M. Salameh, A. Alabdala, S. Alrubaye, A. Alassaf, S. Al-HajAli, R. Al-Wardat, N. Bartolini, G. Bongiovannim, and K. Rajendiran, "Wireless sensor networks for smart cities: Network design, implementation and performance evaluation," *Electronics*, vol. 10, no. 2, p. 218, Jan. 2021, doi: 10.3390/electronics10020218.

[5] L. García, L. Parra, J. M. Jimenez, M. Parra, J. Lloret, P. V. Mauri, and P. Lorenz, "Deployment strategies of soil monitoring WSN for precision agriculture irrigation scheduling in rural areas," *Sensors*, vol. 21, no. 5, p. 1693, Mar. 2021, doi: 10.3390/s21051693.

[6] S. Madhu, S. Padunnavalappil, P. P. Saajlal, V. A. Vasudevan, and J. Mathew, "Powering up an IoT-enabled smart home: A solar powered smart inverter for sustainable development," *Int. J. Softw. Sci. Comput. Intell.*, vol. 14, no. 1, pp. 1–21, May 2022, doi: 10.4018/ijssci.300362.

[7] J. Liang, M. Tian, Y. Liu, and J. Zhou, "Coverage optimization of soil moisture wireless sensor networks based on adaptive Cauchy variant butterfly optimization algorithm," *Sci. Rep.*, vol. 12, no. 1, p. 11687, Jul. 2022, doi: 10.1038/s41598-022-15689-3.

[8] M. Shahidul Islam, M. T. Islam, A. F. Almutairi, G. K. Beng, N. Misran, and N. Amin, "Monitoring of the human body signal through the Internet of Things (IoT) based LoRa wireless network system," *Appl. Sci.*, vol. 9, no. 9, p. 1884, May 2019, doi: 10.3390/app9091884.

[9] U. Musa, S. M. Shah, H. A. Majid, I. A. Mahadi, M. K. A. Rahim, M. S. Yahya, and Z. Z. Abidin, "Design and analysis of a compact dual-band wearable antenna for WBAN applications," *IEEE Access*, vol. 11, pp. 30996–31009, 2023, doi: 10.1109/ACCESS.2023.3262298.

[10] C. G. Christodoulou, Y. Tawk, S. A. Lane, and S. R. Erwin, "Reconfigurable antennas for wireless and space applications," *Proc. IEEE*, vol. 100, no. 7, pp. 2250–2261, Jul. 2012, doi: 10.1109/JPROC.2012.2188249.

[11] H. S. Munawar, "An overview of reconfigurable antennas for wireless body area networks and possible future prospects," *Int. J. Wireless Microw. Technol.*, vol. 10, no. 2, pp. 1–8, Apr. 2020, doi: 10.5815/ijwmt.2020.02.01.

[12] S. M. Shah, M. F. M. Daud, Z. Z. Abidin, F. C. Seman, S. A. Hamzah, N. Katiran, and F. Zubir, "Frequency reconfiguration mechanism of a PIN diode on a reconfigurable antenna for LTE and WLAN applications," *Int. J. Electr. Comput. Eng.*, vol. 8, no. 3, p. 1893, Jun. 2018, doi: 10.11591/ijece.v8i3.pp1893-1902.

[13] B. BharathiDevi and J. Kumar, "Small frequency range discrete bandwidth tunable multiband MIMO antenna for radio/LTE/ISM-2.4 GHz band applications," *Int. J. Electron. Commun.*, vol. 144, Feb. 2022, Art. no. 154060, doi: 10.1016/j.aeue.2021.154060.

[14] P. B. Nikam, J. Kumar, V. Sivanagaraju, and A. Baidya, "Dual-band reconfigurable EBG loaded circular patch MIMO antenna using defected ground structure (DGS) and PIN diode integrated branch-lines (BLs)," *Measurement*, vol. 195, May 2022, Art. no. 111127, doi: 10.1016/j.measurement.2022.111127.

[15] B. R. S. Reddy, N. K. Darimireddy, C.-W. Park, and A. Chehri, "Performance of reconfigurable antenna fabricated on flexible and nonflexible materials for band switching applications," *Energies*, vol. 14, no. 9, p. 2553, Apr. 2021, doi: 10.3390/en14092553.

[16] J. Cui, F.-X. Liu, L. Zhao, and W. Dou, "Textile fixed-frequency pattern-reconfigurable coupled-mode substrate-integrated cavity antenna," *IEEE Antennas Wireless Propag. Lett.*, vol. 21, pp. 1916–1919, 2022, doi: 10.1109/LAWP.2022.3185205.

[17] B. P. Nadh, B. T. P. Madhav, M. S. Kumar, T. A. Kumar, M. V. Rao, and S. S. M. Reddy, "MEMS-based reconfigurable and flexible antenna for body-centric wearable applications," *J. Electromagn. Waves Appl.*, vol. 36, no. 10, pp. 1389–1403, Jul. 2022, doi: 10.1080/09205071.2022.2028682.

[18] N. Hussain, W. A. Awan, S. I. Naqvi, A. Ghaffar, A. Zaidi, S. A. Naqvi, A. Iftikhar, and X. J. Li, "A compact flexible frequency reconfigurable antenna for heterogeneous applications," *IEEE Access*, vol. 8, pp. 173298–173307, 2020, doi: 10.1109/ACCESS.2020.3024859.

[19] F. A. Tahir and A. Javed, "A compact dual-band frequency-reconfigurable textile antenna for wearable applications," *Microw. Opt. Technol. Lett.*, vol. 57, no. 10, pp. 2251–2257, Oct. 2015, doi: 10.1002/mop.29311.

[20] J. Kumar, B. Basu, and F. A. Talukdar, "Modeling of a PIN diode RF switch for reconfigurable antenna application," *Scientia Iranica*, vol. 26, no. 3, pp. 1714–1723, Jan. 2019, doi: 10.24200/sci.2018.20110.

[21] J. Kumar, F. A. Talukdar, and B. Basu, "Frequency reconfigurable E-shaped patch antenna for medical applications," *Microw. Opt. Technol. Lett.*, vol. 58, no. 9, pp. 2214–2217, Sep. 2016, doi: 10.1002/mop.30018.

[22] J. Kumar, B. Basu, F. A. Talukdar, and A. Nandi, "Stable-multiband frequency reconfigurable antenna with improved radiation efficiency and increased number of multiband operations," *IET Microw., Antennas Propag.*, vol. 13, no. 5, pp. 642–648, Apr. 2019, doi: 10.1049/iet-map.2018.5602.

[23] C. Nikolopoulos, A. Baklezos, and C. Capsalis, "Reconfigurable antennas: Theory and techniques—A survey," in *Wideband, Multiband, and Smart Reconfigurable Antennas for Modern Wireless Communications* (Wideband, Multiband, and Smart Reconfigurable Antennas for Modern Wireless Communications). Hershey, PA, USA: IGI Global, 2015, p. 34.

[24] R. Kumar and D. Ritu, "Reconfigurable antenna's: A survey," *Int. J. Eng. Develop. Res.*, vol. 2, no. 3, pp. 3090–3099, 2014.

[25] R. L. Haupt and M. Lanagan, "Reconfigurable antennas," *IEEE Antennas Propag. Mag.*, vol. 55, no. 1, pp. 49–61, Feb. 2013, doi: 10.1109/MAP.2013.6474484.

[26] L. Fuxing, C. Changchun, W. Han, W. Lei, L. Qishuai, A. Qi, and Y. Yintang, "Study on high power microwave nonlinear effects and degradation characteristics of C-band low noise amplifier," *Microelectron. Rel.*, vol. 128, Jan. 2022, Art. no. 114427, doi: 10.1016/j.microrel.2021.114427.

[27] D. M. Pozar, *Microwave Engineering*, 3rd ed. Hoboken, NJ, USA: Wiley, 2009.

[28] N. Ibrahim, R. Tomari, W. N. Wan Zakaria, and N. Othman, "Non-contact heart rate monitoring analysis from various distances with different face regions," *Int. J. Electr. Comput. Eng.*, vol. 7, no. 6, p. 3030, Dec. 2017, doi: 10.11591/ijece.v7i6.pp3030-3036.

[29] Y. Fan, P. Xu, H. Jin, J. Ma, and L. Qin, "Vital sign measurement in telemedicine rehabilitation based on intelligent wearable medical devices," *IEEE Access*, vol. 7, pp. 54819–54823, 2019, doi: 10.1109/ACCESS.2019.2913189.

[30] K. Bhagchandani and D. P. Augustine, "IoT based heart monitoring and alerting system with cloud computing and managing the traffic for an ambulance in India," *Int. J. Electr. Comput. Eng.*, vol. 9, no. 6, pp. 5068–5074, Dec. 2019, doi: 10.11591/ijece.v9i6.pp5068-5074.

[31] S. Misbahuddin, M. M. Ibrahim, A. M. Alnajar, B. Q. Alolabi, and A. F. Ammar, "Automatic patients' vital sign monitoring by single board computer (SBC) based MPI cluster," in *Proc. 2nd Int. Conf. Comput. Appl. Inf. Secur. (ICCAIS)*, May 2019, pp. 1–5, doi: 10.1109/CAIS.2019.8769551.

[32] M. A. Yusof and Y. W. Hau, "Mini home-based vital sign monitor with Android mobile application (myVitalGear)," in *Proc. IEEE-EMBS Conf. Biomed. Eng. Sci. (IECBES)*, Dec. 2018, pp. 150–155, doi: 10.1109/IECBES.2018.8626639.

[33] A. Hodge, H. Humnabadkar, and A. Bidwai, "Wireless heart rate monitoring and vigilant system," in *Proc. 3rd Int. Conf. Converg. Technol. (I2CT)*, Apr. 2018, pp. 1–5, doi: 10.1109/I2CT.2018.8529443.

[34] M. Shu, M. Tang, M. Yang, and N. Wei, "The vital signs real-time monitoring system based on Internet of Things," in *Proc. 4th Int. Conf. Inf. Sci. Control Eng. (ICISCE)*, Jul. 2017, pp. 747–751, doi: 10.1109/ICISCE.2017.160.

[35] R. R. Rajanna, S. Natarajan, and P. R. Vittal, "An IoT Wi-Fi connected sensor for real time heart rate variability monitoring," in *Proc. 3rd Int. Conf. Circuits, Control, Commun. Comput. (I4C)*, Oct. 2018, pp. 1–4, doi: 10.1109/CIMCA.2018.8739323.
[36] K. Kalaithasan, N. A. M. Radzi, and H. Z. Abidin, "Internet of Things application in monitoring sick building syndrome," *Indonesian J. Electr. Eng. Comput. Sci.*, vol. 12, no. 2, p. 505, Nov. 2018, doi: 10.11591/ijeecs.v12.i2.pp505-512.
[37] N. A. Zakaria, F. N. B. M. Saleh, and M. A. A. Razak, "IoT (Internet of Things) based infant body temperature monitoring," in *Proc. 2nd Int. Conf. BioSignal Anal., Process. Syst. (ICBAPS)*, Jul. 2018, pp. 148–153, doi: 10.1109/ICBAPS.2018.8527408.
[38] M. Irmansyah, E. Madona, A. Nasution, and R. Putra, "Low cost heart rate portable device for risk patients with IoT and warning system," in *Proc. Int. Conf. Appl. Inf. Technol. Innov. (ICAITI)*, Sep. 2018, pp. 46–49, doi: 10.1109/ICAITI.2018.8686761.
[39] E. Selem, M. Fatehy, S. M. Abd El-Kader, and H. Nassar, "THE (temperature heterogeneity energy) aware routing protocol for IoT health application," *IEEE Access*, vol. 7, pp. 108957–108968, 2019, doi: 10.1109/ACCESS.2019.2931868.
[40] E. N. Ganesh, "Health monitoring system using raspberry pi and IoT," *Oriental J. Comput. Sci. Technol.*, vol. 12, no. 1, pp. 8–13, Apr. 2019, doi: 10.13005/ojcst12.01.03.
[41] T. Sollu, Alamsyah, M. Bachtiar, and B. Bontong, "Monitoring system heartbeat and body temperature using raspberry Pi," in *Proc. E3S Web Conf.*, vol. 73, 2018, p. 12003, doi: 10.1051/e3sconf/20187312003.
[42] N. S. M. Hadis, M. N. Amirnazarullah, M. M. Jafri, and S. Abdullah, "IoT based patient monitoring system using sensors to detect, analyse and monitor two primary vital signs," *J. Phys., Conf. Ser.*, vol. 1535, no. 1, May 2020, Art. no. 012004, doi: 10.1088/1742-6596/1535/1/012004.
[43] M. Masud, G. S. Gaba, K. Choudhary, M. S. Hossain, M. F. Alhamid, and G. Muhammad, "Lightweight and anonymity-preserving user authentication scheme for IoT-based healthcare," *IEEE Internet Things J.*, vol. 9, no. 4, pp. 2649–2656, Feb. 2022, doi: 10.1109/JIOT.2021.3080461.
[44] J. Wan, M. A. A. H. Al-awlaqi, M. Li, M. O'Grady, X. Gu, J. Wang, and N. Cao, "Wearable IoT enabled real-time health monitoring system," *EURASIP J. Wireless Commun. Netw.*, vol. 2018, no. 1, pp. 1–10, Dec. 2018, doi: 10.1186/s13638-018-1308-x.
[45] M. Masud, G. Muhammad, H. Alhumyani, S. S. Alshamrani, O. Cheikhrouhou, S. Ibrahim, and M. S. Hossain, "Deep learning-based intelligent face recognition in IoT-cloud environment," *Comput. Commun.*, vol. 152, pp. 215–222, Feb. 2020, doi: 10.1016/j.comcom.2020.01.050.
[46] M. M. Khan, T. M. Alanazi, A. A. Albraikan, and F. A. Almalki, "IoT-based health monitoring system development and analysis," *Secur. Commun. Netw.*, vol. 2022, Apr. 2022, Art. no. 9639195, doi: 10.1155/2022/9639195.
[47] V. B. Shalini, "Smart health care monitoring system based on Internet of Things (IoT)," in *Proc. Int. Conf. Artif. Intell. Smart Syst. (ICAIS)*, Mar. 2021, pp. 1449–1453, doi: 10.1109/ICAIS50930.2021.9396019.
[48] M. Saranya, R. Preethi, M. Rupasri, and V. Sundareswaran, "A survey on health monitoring system by using IoT," *Int. J. Res. Appl. Sci. Eng. Technol.*, vol. 6, no. 3, pp. 778–782, Mar. 2018, doi: 10.22214/ijraset.2018.3124.
[49] F. Hirtenfelder, "Effective antenna simulations using CST MICROWAVE STUDIO®," in *Proc. 2nd Int. ITG Conf. Antennas*, Mar. 2007, p. 239, doi: 10.1109/inica.2007.4353972.
[50] M. Nahas, "Design of a high-gain dual-band LI-slotted microstrip patch antenna for 5G mobile communication systems," *J. Radiat. Res. Appl. Sci.*, vol. 15, no. 4, Dec. 2022, Art. no. 100483, doi: 10.1016/j.jrras.2022.100483.
[51] Skyworks Solutions Inc. (1321). *SMP 1321-079LF*. [Online]. Available: https://www.skyworksinc.com/Products/Diodes/SMP1321-Series
[52] Md. A. Towfiq, A. Khalat, S. Blanch, J. Romeu, L. Jofre, and B. A. Cetiner, "Error vector magnitude, intermodulation, and radiation characteristics of a bandwidth- and pattern-reconfigurable antenna," *IEEE Antennas Wireless Propag. Lett.*, vol. 18, pp. 1956–1960, 2019, doi: 10.1109/LAWP.2019.2933379.
[53] S. W. Z. Mahmoud and A. Mahmoud, "Relative intensity noise and nonlinear distortions of semiconductor laser under analog modulation for use in CATV systems," *Int. J. New Horizons Phys.*, vol. 2, no. 2, pp. 37–45, 2015. [Online]. Available: https://naturalspublishing.com/Article.asp?ArtcID=9239
[54] S. Makhsuci and M. Ehsanian, "Oscillation-based test for measuring 1dB gain compression point of power amplifiers," in *Proc. Electr. Eng. (ICEE), Iranian Conf.*, May 2018, pp. 190–195, doi: 10.1109/ICEE.2018.8472454.
[55] N. Muchhal and N. Bhardwaj, "Analysis and measurement technique for 1-dB compression point of single balanced RF mixer," *J. Inf. Eng. Appl.*, vol. 3, no. 6, 2013.
[56] A. Pant, L. Kumar, R. D. Gupta, and M. S. Parihar, "Investigation on non-linear aspects of pattern reconfigurable hexagon shaped planar loop antenna," *IET Microw., Antennas Propag.*, vol. 13, no. 8, pp. 1158–1165, Jul. 2019, doi: 10.1049/iet-map.2018.5344.
[57] R. Gonçalves, P. Pinho, and N. B. Carvalho, "Compact, frequency reconfigurable, printed monopole antenna," *Int. J. Antennas Propag.*, vol. 2012, 2012, Art. no. 602780, doi: 10.1155/2012/602780.
[58] A. W. Pang, S. Bensmida, C. D. Gamlath, and M. J. Cryan, "Non-linear characteristics of an optically reconfigurable microwave switch," *IET Microw., Antennas Propag.*, vol. 12, no. 7, pp. 1060–1063, Jun. 2018, doi: 10.1049/iet-map.2017.0572.
[59] G. A. R. Arroyave, A. Barlabé, L. Pradell, J. L. A. Quijano, B. A. Cetiner, and L. Jofre-Roca, "Design of minimum nonlinear distortion reconfigurable antennas for next-generation communication systems," *Sensors*, vol. 21, no. 7, p. 2557, Apr. 2021, doi: 10.3390/s21072557.
[60] J.-B. Yan, S. Yong, and J. T. Bernhard, "Intermodulation and harmonic distortion in frequency reconfigurable slot antenna pairs," *IEEE Trans. Antennas Propag.*, vol. 62, no. 3, pp. 1138–1146, Mar. 2014, doi: 10.1109/TAP.2013.2294197.
[61] E. A. Banu and V. Rajamani, "Design of online vitals monitor by integrating big data and IoT," *Comput. Syst. Sci. Eng.*, vol. 44, no. 3, pp. 2469–2487, 2023, doi: 10.32604/csse.2023.021332.
[62] S. M. Ali, C. Sovuthy, S. Noghanian, T. Saeidi, M. F. Majeed, A. Hussain, F. Masood, S. M. Khan, S. A. Shah, and Q. H. Abbasi, "Design and evaluation of a button sensor antenna for on-body monitoring activity in healthcare applications," *Micromachines*, vol. 13, no. 3, p. 475, Mar. 2022, doi: 10.3390/mi13030475.
[63] S. J. Chen, D. C. Ranasinghe, and C. Fumeaux, "A robust snap-on button solution for reconfigurable wearable textile antennas," *IEEE Trans. Antennas Propag.*, vol. 66, no. 9, pp. 4541–4551, Sep. 2018, doi: 10.1109/TAP.2018.2851288.
[64] A. Romputtal and C. Phongcharoenpanich, "T-slot antennas-embedded ZigBee wireless sensor network system for IoT-enabled monitoring and control systems," *IEEE Internet Things J.*, vol. 10, no. 23, pp. 20834–20845, Dec. 2023, doi: 10.1109/JIOT.2023.3284005.
[65] K. R. Jha, B. Bukhari, C. Singh, G. Mishra, and S. K. Sharma, "Compact planar multistandard MIMO antenna for IoT applications," *IEEE Trans. Antennas Propag.*, vol. 66, no. 7, pp. 3327–3336, Jul. 2018, doi: 10.1109/TAP.2018.2829533.
[66] M. S. Islam, M. T. Islam, M. A. Ullah, G. K. Beng, N. Amin, and N. Misran, "A modified meander line microstrip patch antenna with enhanced bandwidth for 2.4 GHz ISM-band Internet of Things (IoT) applications," *IEEE Access*, vol. 7, pp. 127850–127861, 2019, doi: 10.1109/ACCESS.2019.2940049.
[67] H. A. Harris, R. Anwar, Y. Wahyu, M. I. Sulaiman, Z. Mansor, and D. A. Nurmantris, "Design and implementation of wearable antenna textile for ism band," *Prog. Electromagn. Res. C*, vol. 120, pp. 11–26, 2022, doi: 10.2528/pierc22022501.
[68] H. Xiaomu, S. Yan, and G. A. E. Vandenbosch, "Wearable button antenna for dual-band WLAN applications with combined on and off-body radiation patterns," *IEEE Trans. Antennas Propag.*, vol. 65, no. 3, pp. 1384–1387, Mar. 2017, doi: 10.1109/TAP.2017.2653768.

UMAR MUSA (Student Member, IEEE) received the bachelor's degree in electrical engineering from Bayero University Kano, Nigeria, in 2012, and the M.Eng. degree in electronic and telecommunication engineering from Universiti Teknologi Malaysia (UTM), Malaysia, in 2016. He is currently pursuing the Ph.D. degree with the Department of Communication Engineering, Faculty of Electrical and Electronic Engineering, Universiti Tun Hussein Onn Malaysia (UTHM). He is also a Lecturer with the Department of Electrical Engineering, Bayero University Kano. His research interests include, but not limited to, design of RF and microwave devices and active antennas measurement. He has been a member of the Council for the Regulation of Engineering in Nigeria, since 2019.

SHAHARIL MOHD SHAH received the B.Eng. degree in microwave and communication from Multimedia University (MMU), in 2002, the M.Sc. degree in microwave engineering and wireless subsystems design from the University of Surrey, U.K., in 2004, and the Ph.D. degree in communication engineering from the University of Birmingham, U.K., in 2016. He is currently a Senior Lecturer with the Department of Communication Engineering, Faculty of Electrical and Electronic Engineering, Universiti Tun Hussein Onn Malaysia (UTHM). His research interests include, but not limited to, design of microwave devices, active antennas measurement, and nonlinear characterization of active devices.

HUDA A. MAJID (Member, IEEE) received the B.Eng. degree in electrical engineering (telecommunication) and the M.Eng. and Ph.D. degrees in electrical engineering from Universiti Teknologi Malaysia, in 2007, 2010, and 2013, respectively. He is currently a Lecturer with the Department of Electrical Engineering Technology, Faculty of Engineering Technology, Universiti Tun Hussein Onn Malaysia. He has published over 90 papers in journals and conferences. His research interests include the areas of design of microstrip antennas, small antennas, reconfigurable antennas, metamaterial's structure, metamaterial antennas, and millimetre wave antennas.

ISMAIL AHMAD MAHADI (Graduate Student Member, IEEE) received the bachelor's and M.Eng. degrees in electrical engineering from Universiti Tun Hussein Onn Malaysia (UTHM) in 2023. He is a staff with the Faculty of Exact and Applied Science, University of N'Djamena, Chad. His research interests include wireless power transfer and control system for AC high-frequency inverters.

MOHAMAD KAMAL A. RAHIM (Senior Member, IEEE) received the B.Eng. degree in electrical and electronic engineering from the University of Strathclyde, U.K., in 1987, the M.Eng. degree in science from the University of New South Wales, Australia, in 1992, and the Ph.D. degree in electrical engineering from the University of Birmingham, U.K., in 2003. From 1987 to 1989, he was a Management Trainee with Sime Tyres, Mergong, Alor Setar, Kedah, and the Production Supervisor of Sime Shoes, Kulim, Kedah. He joined the Department of Communication Engineering, Faculty of Electrical Engineering, Universiti Teknologi Malaysia, Kuala Lumpur, as an Assistant Lecturer, in 1989. After receiving the master's degree, he was appointed as a Lecturer with the Faculty of Electrical Engineering. He was appointed as a Senior Lecturer, in 2005. He was appointed as an Associate Professor with the Faculty. He is currently a Professor of RF and antenna with the Faculty of Electrical Engineering, Universiti Teknologi Malaysia. His research interests include design of dielectric resonator antennas, microstrip antennas, small antennas, microwave sensors, RFID antennas for readers and tags, multifunction antennas, microwave circuits, EBG, artificial magnetic conductors, metamaterials, phased array antennas, computer-aided design for antennas, and design of millimeter frequency antennas.

MUHAMMAD SANI YAHYA (Graduate Student Member, IEEE) received the B.Eng. degree in electrical and electronics engineering from Abubakar Tafawa Balewa University (ATBU), Bauchi, Nigeria, in 2010, and the M.Eng. degree in electronic and telecommunication engineering from Universiti Teknologi Malaysia (UTM), in 2016. He is currently pursuing the Ph.D. degree with the Department of Electrical and Electronics Engineering, Universiti Teknologi PETRONAS (UTP), Malaysia. He has published some articles in both local and international journals and have attended several both local and international conferences. His research interests include RF and microwave: antenna design and characterizations.

ZUHAIRIAH ZAINAL ABIDIN (Senior Member, IEEE) received the Ph.D. degree from the University of Bradford, U.K., in 2011. She is currently an Associate Professor and the Head of the Advanced Telecommunication Research Center (ATRC), Universiti Tun Hussein Onn Malaysia. She has authored and coauthored numbers of journals and proceedings. Her research interests include MIMO antenna, printed microstrip antenna, wearable antennas, metamaterial resonator, electromagnetic bandgap (EBG) for wireless and mobile, and high-speed digital circuit's applications.